A Study of the Effect of Thread Forming on the Susceptibility of Precipitation Hardened Ni-Based Alloy Fasteners to Hydrogen Embrittlement

API TECHNICAL REPORT 21D

FIRST EDITION, XXXXXXXXXXXXXXXXX 202X

Introduction

This study was completed in response to recommendations by API to investigate and quantify the relative hardness of threaded precipitation hardened Ni-based alloys (PHNAs), by both machined and cold rolled methods. This study also aligns with recommendations issued by the API Multi Segment Task Group on Bolting Failures (February 29, 2016), where it was concluded that "Product subcommittees should review and consider…resolving existing conflicting properties specified in product specifications…". The information in this technical report has not been readily available as existing public or industry data.

Industry specifications often require hardness testing of PHNAs used for bolting in their final process condition, i.e., after all heat treatments, secondary processing, and machining. Threads, however, can be cold rolled into the product, which is a form of secondary processing that cannot be routinely tested for material properties. Further, cold rolling is a form of strain hardening which increases hardness in the affected area. This can result in conflicting requirements, or industry specification interpretation differences of requirements, which can be problematic with respect to specification compliance.

Due to the general nature of hardness and microstructure impact on susceptibility of materials to hydrogen charging environments, additional hydrogen embrittlement incremental step load testing (i.e., a fracture mechanics-based approach) was also performed. Novel specimen geometries were used for accurate assessment of both machined and cold rolled threads, and the results compared to bulk material properties.

The PHNAs studied in this program were alloy 718-120k (UNS N07718), alloy 718-150k (UNS N07718), alloy 725-120k (UNS N07725), and alloy 945-120k (UNS N09945). All materials tested were manufactured in compliance with API 6ACRA 1st Edition.

1 Scope

This report quantifies the hardness profile of both machined and rolled threads in PHNAs, studies the effects of both machined and rolled threads on hydrogen induced stress cracking (HISC) susceptibility in relevant PHNAs, tests these PHNA grades used for bolting per API Standards requirements, and provides guidance for the use of the selected testing methodology and resultant test data in the Petroleum and Natural Gas industry.

2 Normative References

There are no referenced documents that are indispensable for the application of this document.

3 Terms, Definitions, and Abbreviations

3.1 Terms and Definitions

For the purposes of this document, the following terms and definitions apply.

3.1.1
Damage Tolerance Index
DTI
A calculated parameter which uses both fracture mechanics and mechanical properties to assess the critical defect size under a given stress intensity for a given material.

3.1.2
Hydrogen susceptibility ratio
Hsr
A calculated parameter which uses both applied stresses and mechanical properties to assess the magnitude of effect a specific thread or surface geometry has on the hydrogen embrittlement susceptibility of a given material.

3.1.3
K_{Ic}
The critical stress intensity under Mode I loading conditions at which the onset of crack growth begins.

NOTE See ASTM E399 for additional information.

3.2 Abbreviations

For the purposes of this document, the following abbreviations apply.

CP Cathodic Protection

CT Cut Threads

CTOD	Crack Tip Opening Displacement
CVN	Charpy V-Notched
DTI	Damage Tolerance Index
DTI_p	The Damage Tolerance Index of a given specimen with a threaded geometry (i.e. root radius) exposed to a given environment.
EDM	Electric Discharge Machining
EHE	External (or Environmental) Hydrogen Embrittlement
FFS	Fast Fracture Strength
HE	Hydrogen Embrittlement
HISC	Hydrogen Induced Stress Cracking
Hsr	Hydrogen susceptibility ratio
HV	Vickers Hardness Scale
IHE	Internal Hydrogen Embrittlement (during manufacturing process)
ISL	Incremental Step Load Test
KI_C	The critical stress intensity under Mode I loading conditions at which the onset of crack growth begins.
KI_p	The critical stress intensity under Mode I loading conditions of a given specimen with a threaded geometry (i.e. root radius).
MTR	Material Test Report
P_{EHE}	The threshold load of a given specimen due to EHE
P_{MAX}	Maximum attainable load of a given specimen before failure
PHNA	Precipitation Hardened Nickel-based Alloy
SCE	Saturated Calomel Electrode
SEN(B)	Single-Edge Notched specimens, tested in Bending
SG	Side Groove
RT	Rolled Threads
UTS	Ultimate Tensile Strength
YS	Yield Strength

4 Test Plan

4.1 Test Protocols and Environment

Multiple lots of bolts made of materials as shown in Table 1 were submitted for testing to evaluate the effect of thread forming processes (cut vs. rolled) on hardness and bolting susceptibility to HISC due to EHE while in simulated service conditions. General assessment of the alloys consisted of the following:

a) Cross-section microhardness surveys were performed on specimens from each alloy and heat treatment condition, with both cut and rolled threads.

b) Fracture toughness values were measured for each alloy and heat treatment condition.

c) Threshold incremental step load cracking values in a 3.5% NaCl solution with simulated CP were measured for each alloy and heat treatment condition, with both cut and rolled threads. Novel specimen geometry was determined such that an as-manufactured thread acted as the stressed notch.

All testing was performed on rigid, displacement controlled four-point bend frames that were programmed to increase load incrementally in a stair-step pattern to vary the strain rate at the specimen notch between 10^{-4} and 10^{-9} in/in/s (mm/mm/s).

Initial FFS and Fracture Toughness tests were performed in air to establish baseline values. Subsequent specimens subjected to EHE testing were immersed in an aqueous 3.5% NaCl solution with an imposed potential of -1.2V_{SCE} (roughly equivalent to -1.15$V_{Ag/AgCl\text{-}Seawater}$), which is more than typical subsea cathodic protection to maintain a conservative approach. The potential was controlled with a reference electrode that was positioned with its tip within 1 in. (25.4 mm) of the specimen being tested. A length of platinum wire was used as an auxiliary electrode and positioned on the opposite end of the environmental chamber. All testing was performed at ambient temperature (75°F/25°C) and pressure (1 atm./101.3 kPa).

4.2 Test Materials

The PHNAs studied in this program were 718-120k (UNS N07718), alloy 718-150k (UNS N07718), alloy 725-120k (UNS N07725), and alloy 945-120k (UNS N09945), as identified per API 6ACRA. Upon receipt, hardness measurements were taken at the core of each bolt. The mechanical properties and chemical compositions of the bolts were compiled from the material test reports (MTRs) and are listed in Table 1 and Table 2, respectively. All materials were tested in the solution annealed and age hardened condition and originally certified to API 6ACRA, 1st Edition requirements.

Table 1–Mechanical Properties of Tested Materials

Material Designation	Heat ID	Bar Diameter in. (mm)	Yield Strength ksi (MPa)	Tensile Strength ksi (MPa)	Elongation (%)	Reduction of Area (%)	Average Hardness[a] (HRC)	Average Grain Size[a]
718-120k	1	2 (50.8)	138 (951.5)	185 (1,275.5)	31	44	37	4
	2	2 (50.8)	129 (889.4)	175 (1,206.6)	31	46	37.6	4
718-150k	1	2 (50.8)	155.0 (1,068.7)	184.6 (1,272.8)	28	55	42.3	3.5
	2	2 (50.8)	153.3 (1,056.9)	182.7 (1,259.7)	29	54	42.6	3.5
725-120k (2020)[b]	1	2 (50.8)	135 (930.8)	183 (1,261.7)	31	49	40.6	3.7
	2	2.25 (57.2)	132 (910.1)	180 (1,241.1)	31	45	39.7	3.7
725-120k (2022)[b]	1	2 (50.8)	120.5 (830.8)	171.0 (1,179.0)	36	46	37.8	2.5
	2	2 (50.8)	131.5 (906.7)	177.8 (1,225.9)	37	55	42	3.3
	3	2 (50.8)	125.6 (866.0)	178.7 (1,232.1)	33	43	39.6	3
945-120k	1	1.4 (35.6)	130 (896.3)	165 (1,137.6)	33	50	36.7	3.5

FOOTNOTE

[a] Average hardness and average grain size are calculated from the cross-section hardness and grain size values reported on the original MTRs.

[b] Alloy 725-120k was tested in both 2020 and 2022. See 6.4.

Table 2–Chemical Composition (wt. %) of Tested Materials

Material Designation	718-120k		718-150k		725-120k (2020)		725-120k (2022)			945-120k
Heat ID	1	2	1	2	1	2	1	2	3	1
C	0.016	0.024	0.012	0.014	0.014	0.014	0.007	0.005	0.007	0.013
Mn	0.08	0.06	0.09	0.08	0.05	0.10	0.04	0.03	0.04	0.06
Si	0.06	0.06	0.07	0.07	0.06	0.14	0.05[a]	0.05[a]	0.05[a]	0.08
P	0.009	0.008	0.007	0.008	0.003	0.006	0.005[a]	0.005[a]	0.005[a]	0.008
S	0.0005[a]	0.0005[a]	0.0004	0.0005	0.0005[a]	0.0005[a]	0.0005	0.0005	0.0005	0.001
Cr	18.3	18.4	17.89	17.65	21.0	21.1	21.78	21.58	21.64	20.7
Ni	52.9	52.8	53.8	54.9	57.6	58.0	57.39	58.10	57.56	47.1
Mo	2.90	2.95	2.96	3.02	8.01	8.05	8.14	7.55	8.08	3.22
Cu	0.06	0.05	0.05	0.07	0.02	0.05	0.02	0.07	0.02[a]	2.05
Co	0.36	0.31	0.32	0.38	0.02	0.08	0.05[a]	0.16	0.29	0.2
Sn	0.0011	0.0020	0.0010[a]	0.0015	0.0019	0.0018	0.0010[a]	0.0010[a]	0.0010[a]	NR[b]
Al	0.50	0.50	0.46	0.50	0.19	0.17	0.29	0.26	0.27	0.19
Ti	0.98	0.97	0.96	0.94	1.24	1.28	1.51	1.58	1.50	1.6
Nb (Cb)	4.97	5.06	4.96	4.95	3.40	3.40	3.45	3.44	3.46	3.13
Ta	0.01	0.01[a]	0.020[a]	0.020[a]	0.01	0.01	0.020[a]	0.020[a]	0.020[a]	0.01[a]
Se	0.0003[a]	0.0003[a]	0.0003[a]	0.0003[a]	0.0003[a]	0.0003[a]	0.0004	0.0003[a]	0.0003[a]	NR[b]
Mg	0.0041	0.0043	0.0015	0.0012	0.0011	0.018	0.0010	0.0013	0.0015	0.0008
B	0.0041	0.0037	0.0027	0.0029	0.0028	0.0025	0.0010[a]	0.0031	0.0010[a]	0.0016
Nb+Ta	4.98	5.06	4.98	4.97	3.41	3.41	3.47	3.46	3.48	3.1
Ni+Co	NR[b]	NR[b]	NR[b]	NR[b]	NR[b]	NR[b]	NR[b]	NR[b]	NR[b]	47.4
Bi	0.00003[a]	0.00003[a]	0.00003[a]	0.00003[a]	0.00003[a]	0.00003[a]	0.00003[a]	0.00003[a]	0.00003[a]	NR[b]
Ca	0.0002	0.0003	0.0003[a]	0.0003[a]	0.0010[a]	0.0010[a]	0.0003[a]	0.0002[a]	0.0002[a]	NR[b]
Fe	18.38	18.55	18.31	17.36	8.13	7.54	7.22	7.17	7.08	21.76
Pb	0.0003[a]	0.0003[a]	0.0003[a]	0.0003[a]	0.0003[a]	0.0003[a]	0.0003[a]	0.0003[a]	0.0003[a]	NR[b]
N	0.0061	0.0085	0.005	0.005	NR[b]	NR[b]	NR[b]	NR[b]	NR[b]	0.0054
O	0.001[a]	0.001[a]	0.0004	0.0003	NR[b]	NR[b]	NR[b]	NR[b]	NR[b]	0.0007

FOOTNOTE

[a] Value listed is the lowest resolvable limit by testing equipment on original MTR; actual value is lower than what is shown.

[b] NR indicates “Not Reported” on MTR

4.3 Specimen Preparation

4.3.1 Threading Details

Threading was performed on all materials in the solution annealed and age hardened condition, to ensure the highest thread hardness possible and maintain test conservatism. Both roll thread and cut thread samples were manufactured so as to achieve a UNR thread form, in compliance with ASME B1.1, for each nominal bar diameter shown in Table 1. A UNR-2A thread form was selected because it is a common thread geometry for pressure-containing and closure bolting in the Petroleum and Natural Gas industry and further establishes a notch-type geometry. Discreet bolting samples from each material were separately roll threaded and cut threaded. Roll threading was performed in a single pass on a two-roll thread

rolling machine using a thru-feed process. Cut threading was performed on a single-point CNC lathe. Post-threading dimensional inspection was performed in compliance with ASME B1.3 system 21. Additional inspection included both visual examination and liquid penetrant testing to confirm no thread root indications were present before specimens were extracted.

4.3.2 Specimen Extraction Plan

From each of the full-sized bolts, a minimum of three modified ASTM F519 type 1e Charpy-sized specimens at 0.4 in. x 0.4 in. x 2.25 in. (10 mm x 10 mm x 55 mm) were removed from the outer diameter, as seen in Figure 1, to determine the effective threshold stress intensity of the material with a given thread geometry. In the center of each specimen's gauge section, a 0.75 in. (19 mm) section of threads was left intact. The remaining threads on either side of the gauge length were machined such that a flat, square cross-section was achieved.

Figure 1–Example of specimen extraction locations from threaded product

Additionally, from the center of each bolt as seen in Figure 1, a final 0.4 in. x 0.4 in. x 2.25 in. (10 mm x 10 mm x 55 mm) specimen was removed with a 0.1" (2.54 mm) deep EDM slot in its center to measure CTOD as an estimate of fracture toughness. These specimens were fatigue pre-cracked to a thickness ratio, a/W, of approximately 0.50 prior to being tested in accordance with ASTM E1290.

Vickers microhardness testing was performed in accordance with ASTM E384. For alloys 718-120k and 718-150k, the microhardness profiles were performed on polished cross-sections with a consistent spacing of 0.008 in. (200 microns) between each measurement until mid-radius. For alloys 725-120k and 945-120k, 0.008 in. (200 microns) spacing was maintained until a depth of 0.31 in. (8 mm), and then increased to 0.016 in. (400 microns) until mid-radius as seen in Figure 2. All microhardness tests were performed using a 500g load. Hardness testing was not performed on alloy 725-120k from 2020.

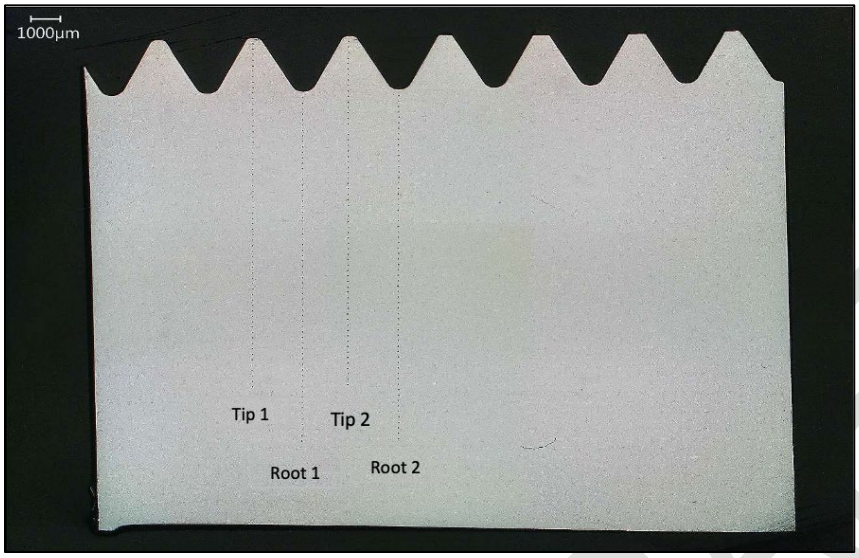

Figure 2–Example of the thread root and thread tip microhardness traverses performed

4.3.3 Specimen Geometry Selection

Preliminary testing on alloy 718-120k was performed using smooth sided specimens. Although the data initially appeared to be acceptable to the requirements in ASTM F1624, visual examination revealed that cracking initiated at the root of multiple threads, as observed in the left image in Figure 3. This made the behavior of any single thread unclear and can lead to lower sensitivity during testing.

Additional preliminary specimens were extracted; however, 45° side-grooves, with a depth of 0.12 in. (3 mm) per groove, were added. Side-grooves normal to the root of the center thread and along the side of each specimen induce plane strain conditions and limit crack growth to a single thread root[1], as observed in the right image in Figure 3. This was confirmed when examined using stereo microscopy at low magnification. Each side-groove was made by electric discharge machining most of the notch and then a final light grind of the area until the proper depth had been achieved. Light grinding was used to remove any heat affected zone from the EDM process, to minimize the risk of excessive work hardening, and to limit any residual stresses, all of which could affect the observed fracture toughness. The samples with side grooves showed higher sensitivity during testing and more reliable crack formation in a single location, because of the restricted plastic flow at the thread root[2].

Based on these observations, the side-groove constrained specimen geometry was selected for testing of all materials. Figure 4 shows a side-groove constrained specimen after ASTM F1624 testing. From the image, while minor yielding can be observed within the threads adjacent to the constrained thread root, crack initiation was confirmed as focused to the thread root of interest.

NOTE: The practice of adding side-grooves to specimens to control crack growth is a common practice allowed by ASTM E1820.

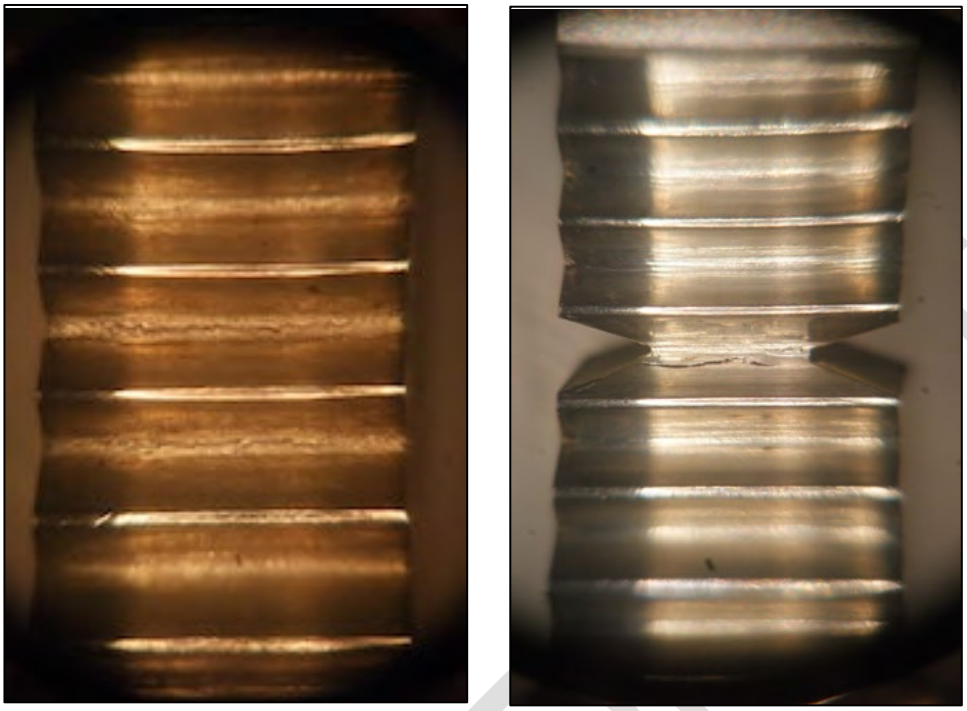

Figure 3- Smooth-sided threaded specimen (left) versus a side-groove constrained threaded specimen (right) after testing. 25x magnification.

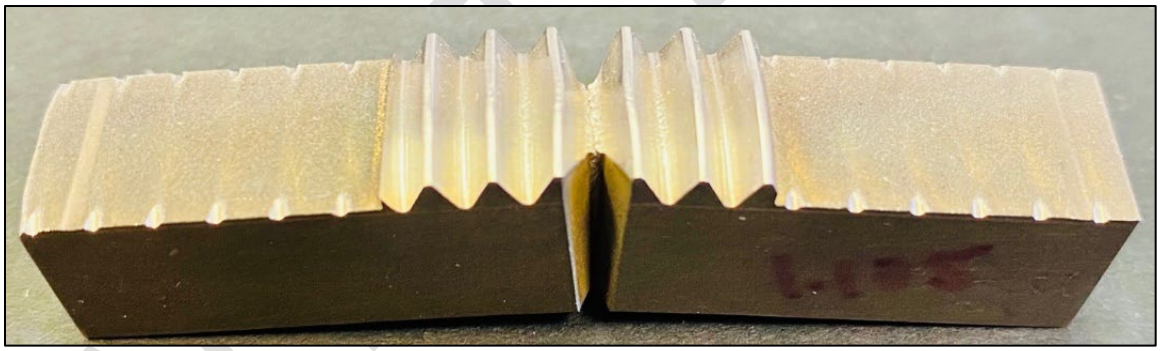

Figure 4-Image of a full side-groove constrained specimen after testing. 3x magnification.

4.4 Incremental Step Load Test Procedure

From each heat, an initial threaded specimen taken from the OD of each bolt was subjected to FFS testing in air at strain rates in accordance with ASTM E8 which are sufficiently rapid to prevent any possible diffusion of hydrogen to regions of high local stress. Results from FFS testing serve as the baseline for determining the maximum load attainable by the specimens from each lot without any effect of hydrogen (i.e. P_{MAX}).

For EHE tests, specimens were subjected to step loading in a 3.5% NaCl solution under four-point bending per ASTM F1624 at progressively decreasing strain rates. The initial target load is determined from the FFS specimen results for the first step loading specimen ($P_{Target} = P_{MAX}$). The step size for the initial ISL test is 1/20th of the target load value, and 20 steps are performed to reach the target load or until cracking initiates. All subsequent samples from the same lot were given a target load based on the load at which cracking initiated on the prior test. The threshold stress intensity for subcritical crack growth due to hydrogen embrittlement (i.e. $KI_{p\text{-}EHE}$) is determined when specimens tested at progressively decreasing strain rates reach an invariant threshold.

NOTE For some of the 2020 testing, the step loading started at 50% of the designated target load to bypass the initial steps where cracking was not expected to occur.

The SEN(B) specimens taken from the bolt center were given a sharp fatigue pre-crack for fracture toughness testing in accordance with ASTM E1290. The specimens were attached to the CTOD gauge using knife-edge fixturing on both sides of the notch and were tested in air to measure CTOD as an estimate of KI_c. An example of CTOD test setup can be seen in Figure 5. Test data was checked using criteria outlined in ASTM E399 for plane strain fracture toughness conditions—no specimens tested were found to meet all plane strain conditions, therefore all fracture toughness values were derived from CTOD measurements.

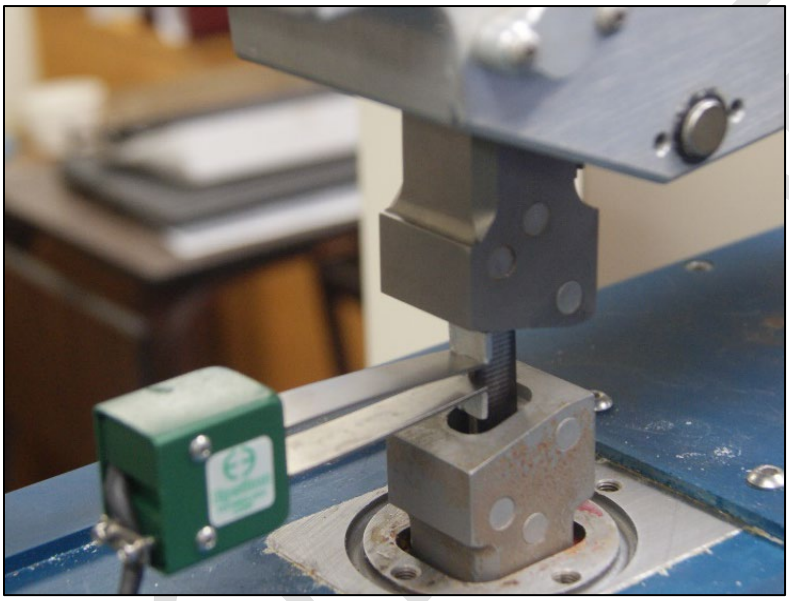

Figure 5- Example of CTOD testing of SEN(B) specimens to determine fracture toughness of material

5 Testing Results

5.1 Hardness Testing Results

The average Vickers (HV) microhardness testing results can be seen in Table 3, which provides an overall summary of the hardness values obtained within the base PHNA and the work hardened zones of both cut and rolled threads.

Table 3-Average Vickers (HV) Microhardness Results for Cut and Rolled Threads

Material Designation	Thread Type	Average Base Material Hardness (HV)	Average Thread Body Hardness (HV)	Average Thread Root Hardness (HV)
718-120k	Cut	421	419	425
	Rolled	403	511	474
718-150k	Cut	425	450	460
	Rolled	433	516	517
725-120k (2022)	Cut	413	438	425
	Rolled	425	570	472
945-120k	Cut	413	411	410

	Rolled	416	506	430

The average base metal hardness was determined from all hardness values at 0.16 in. (4 mm) depth or further from the threaded surfaces. The 718-150k data shown were determined from all base metal hardness values at 0.31 in. (8 mm) depth or further from the threaded surfaces, since the work hardened zones extended deeper into the base material. The average thread body and thread root hardness values were taken within 0.06 in. (1.4 mm), inclusive, of the threaded surfaces. Figure 6 and Figure 7 detail the full Vickers (HV) microhardness profiles for cut and rolled threads, respectively. In all microhardness profiles, the values are charted as a function of absolute distance from the surface.

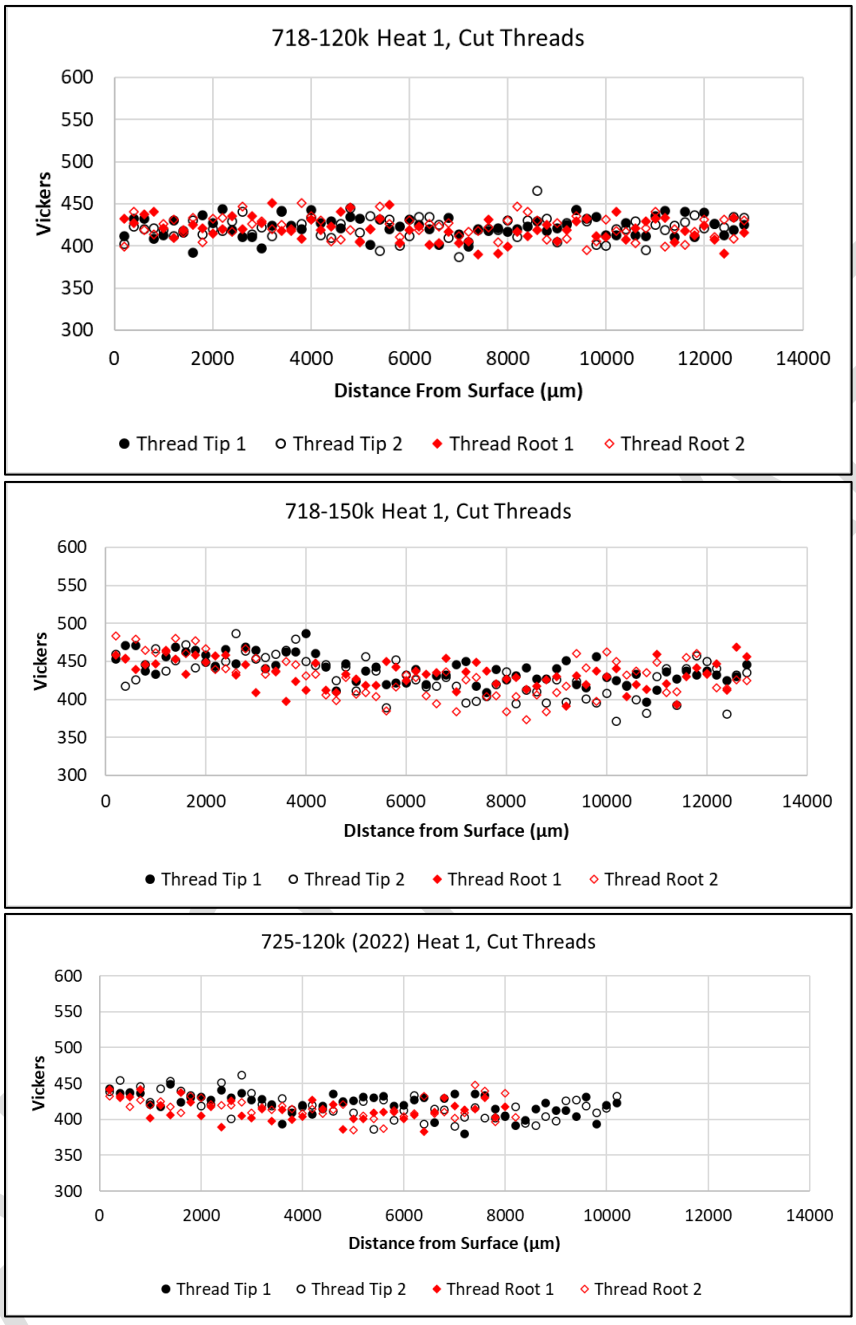

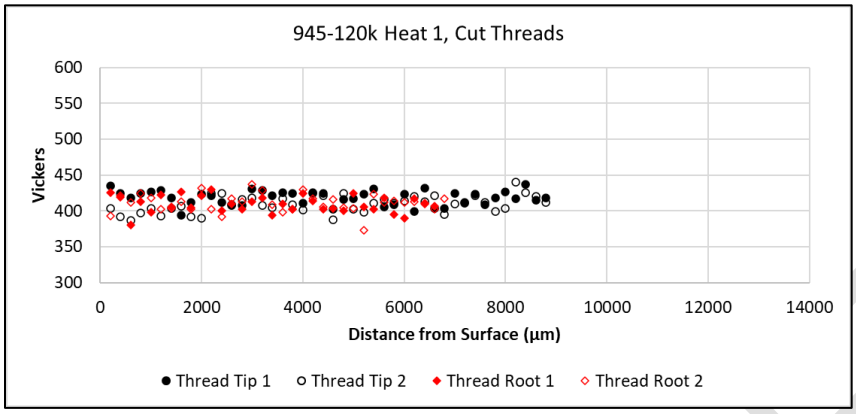

Figure 6- Vickers (HV) microhardness testing of cut threads for each alloy.

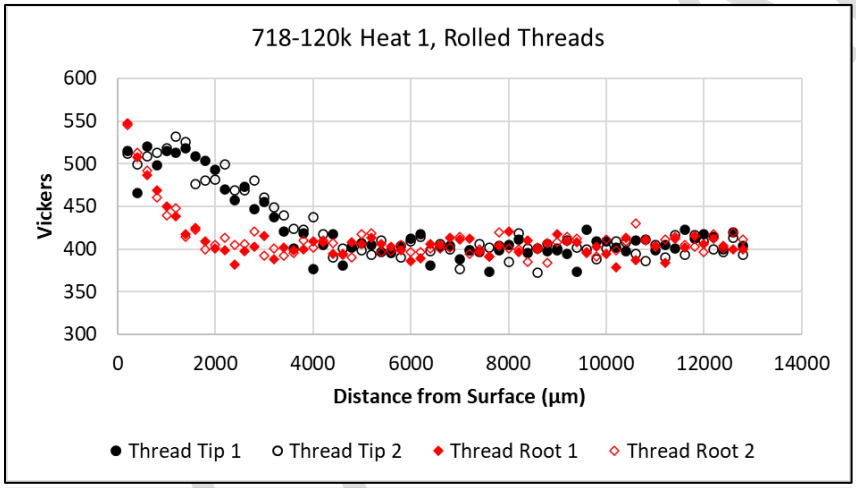

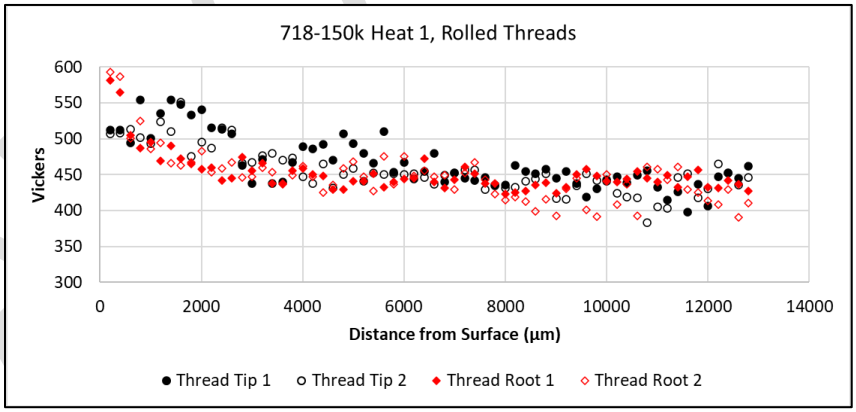

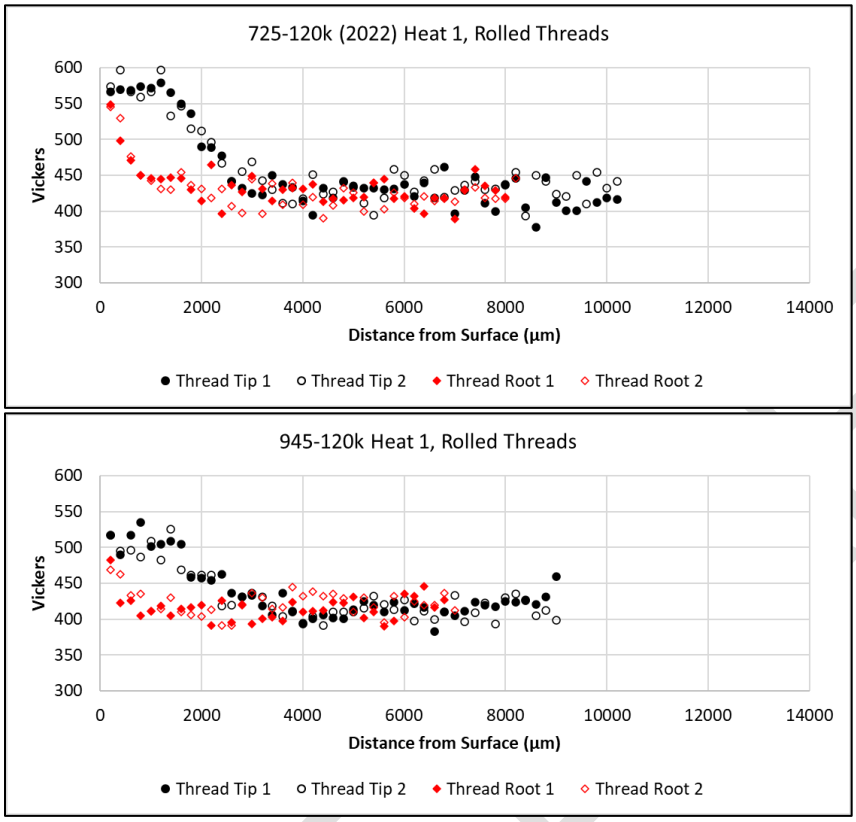

Figure 7- Vickers (HV) microhardness testing of rolled threads for each alloy.

5.2 EHE Testing Results

Results of the EHE testing on the bolt specimens can be seen in Table 4. The lowest stress intensity measured on the specimen from each lot tested is reported as the threshold stress intensity in the table. All ISL testing per ASTM F1624 was performed in a 3.5%NaCl solution. Specimens tested with simulated CP were at an applied potential of -1.2V_{SCE} (roughly equivalent to -1.15$V_{Ag/AgCl\text{-}Seawater}$).

Table 4- Results of fracture toughness testing of all alloys with both cut and rolled threads.

Material Type	Heat ID	Thread Type	Material Fracture Toughness KI_{CTOD} (ksi√in)	Thread Fracture Toughness $KI_{\rho\text{-}MAX}$ (ksi√in)	Thread Fracture Toughness w/ CP $KI_{\rho\text{-}EHE}$ (ksi√in)	%FFS ($KI_{\rho\text{-}EHE}$ / $KI_{\rho\text{-}MAX}$)
718-120k	1	Cut	197.0	127.8	125.8	0.98
		Rolled	197.0	129.5	108.2	0.84
	2	Cut	180.8	124.5	117.2	0.94
		Rolled	180.8	122.1	110.1	0.90
718-150k	1	Cut	206.7	144.6	137.0	0.95
		Rolled	206.7	144.0	114.0	0.79
	2	Cut	227.6	139.4	132.5	0.95
		Rolled	227.6	140.9	117.0	0.83

725-120k (2020)	1	Cut	260.5	132.3	102.3	0.77
		Rolled	260.5	126.8	97.9	0.77
	2	Cut	250.0	126.5	104.3	0.82
		Rolled	250.0	129.5	92.6	0.72
725-120k (2022)	1	Cut	191.7	121.5	36.3	0.30
		Rolled	206.8	125.2	43.5	0.35
	2	Cut	344.0	130.4	88.6	0.68
		Rolled	252.7	131.0	52.6	0.40
	3	Cut	221.1	121.7	30.3	0.25
		Rolled	227.0	128.6	35.0	0.27
945-120k	1	Cut	224.8	107.0	107.0	1.0
		Rolled	224.8	123.7	84.5	0.68

6 Discussion and Observations

6.1 Observations on Hardness Testing

Rolled threads showed a 90-145 HV increase in the thread body, and a 14-85 HV increase in the thread root. Depth of hardness increase was generally within 0.16 in. (4 mm) of the threaded surface, with peak hardness values observed between 0.05 in. (1.2 mm) and 0.06 in. (1.6 mm) from the threaded surface. Cut threads showed a 0-25 HV increase in the thread body, and 0-35 HV increase in the thread root. Depth of hardness increase is shallow and generally within 0.02 in. (0.5 mm) of the threaded surface.

Hardness distribution in the rolled thread profiles, i.e. higher in thread body and lower in thread roots, suggests the formation of threads is by predominantly lateral/shear forces to form the thread body, rather than thread root formation by normal compression of the outer diameter surface. In other words, by cross-section, surface material is primarily compressed into thread “peaks” which results in secondary formed and iterative thread root “valleys”. It is likely thread roots contain helically distributed residual tensile stresses which balance the residual compressive stresses contained in the thread body. Residual stress testing of threaded materials is recommended to characterize the expected strain fields in relation to HISC performance.

For rolled threads, the depth of hardness increase into the base material was dependent on the initial base material strength; with shallower depths of hardness increase at lower base metal strengths and vice versa. Whereas for cut threads, a moderately higher hardness increase range in the thread root can be contributed from tooling forces which are normal to the thread root area during thread cutting operations.

6.2 Observations on Critical Stress Intensity

While thread rolling did appear to provide a marginal increase to the $KI_{\rho\text{-}MAX}$ values, the rolled thread specimens were slightly more susceptible to EHE than the cut thread specimens. Figure 8 is a graphical representation of the critical stress intensity and ISL values across all grades and heats. Except for alloy 725-120k (2022) (see 6.4 for additional microstructural discussion), cut thread specimens were found to have higher threshold $KI_{\rho\text{-}EHE}$ values universally across all alloys and heats. While in many cases, the differences between rolled and cut threads were marginal, thread rolling had a particularly large effect on both alloy 718-150k alloy 945-120k with maximum differences of 23.0 ksi$\sqrt{in}$ and 22.5 ksi$\sqrt{in}$, respectively, between the rolled and cut threads. Interestingly, microhardness readings of alloy 945-120k appeared to show the lowest peak thread root hardness for all rolled thread specimens.

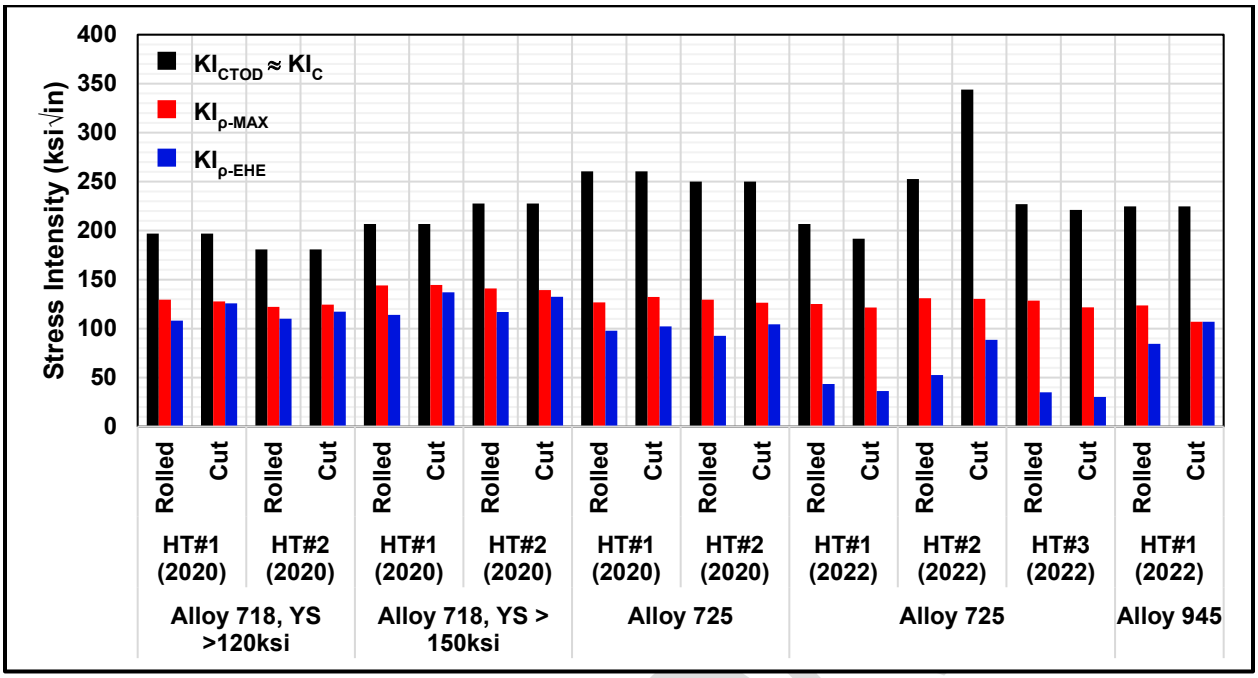

Figure 8- Results of stress intensities for base alloys and for cut and rolled threads.

Alloy 718-150k was found to have the highest threshold for the onset of subcritical crack growth, with peak $KI_{\rho\text{-}EHE}$ for cut and rolled threads measuring 137.0 ksi√in and 132.5 ksi√in, respectively. Alloy 725-120k (2022) was the most susceptible to EHE with $KI_{\rho\text{-}EHE}$ measuring as low as 30.3 ksi√in.

Alloy 725-120k (2020) Heat 1 was found to have the highest fracture toughness of all lots with a fracture toughness measurement of 260.5 ksi√in. Some irregularities in the load profile for alloy 725-120k (2022) Heat 2 were found which may have resulted in erroneously high KI_{CTOD} measurements (>300 ksi√in).

6.3 Observations on Fracture Strength Ratios

To normalize threshold data across all bolts with differing fracture toughness, the %FFS was calculated by taking the ratio of the threshold stress intensity with simulated CP ($KI_{\rho\text{-}EHE}$) and the maximum stress intensity ($KI_{\rho\text{-}MAX}$) attained during the FFS test. Figure 9 is a graphical representation of %FFS for all alloys and heats. As discussed previously, thread rolling was found to have the greatest impact on alloy 945-120k with the rolled threads only achieving 68% of the original FFS, while the cut threads showed 91% FFS when subjected to ISL testing with CP. The susceptibilities of both alloy 725-120k (2020) and alloy 725-120k (2022) can be more clearly visualized when %FFS is plotted. The cut thread specimens from alloy 725-120k (2022) Heat 3 were found to only reach a load 25% of their measured fracture strength when exposed to CP conditions. The next largest decrease in performance of the other alloys is the alloy 945-120k rolled thread specimens which reached a threshold that was 68% of its measured fracture strength.

Cut thread specimens from alloy 718-120k Heat 1 and alloy 945-120k Heat 1 reached a threshold that was either near to or at the measured fracture strength, meaning that there was no measurable degradation in performance when exposed to CP. Furthermore, while multiple conditions had specimens with cut threads that were able to reach thresholds more than 90% of their measured FFS, no specimens with rolled threads were able to surpass that point. ASTM F519 notes that completely un-embrittled Type 1a.1 notched specimens can fail as low as 90% of their certified fracture strength when step loaded. This level can be used as a helpful limit to quickly screen for materials with exceptionally low susceptibility to EHE under the given conditions. This does not mean that materials with thresholds lower than 90% of the measured FFS cannot be or even should not be used in service, however additional variables may need to be considered to determine acceptability in each case. Due to testing of only one heat of alloy 945-120k, it cannot be ascertained if this is indicative of general alloy performance.

The use of %FFS as an initial screening method for general sensitivity of threaded specimens to CP environment can be useful to determine if further testing or study is necessary. For example, if %FFS is lower than 90% or an alternative defined criterion, DTI and Hsr can be useful tools for design criteria.

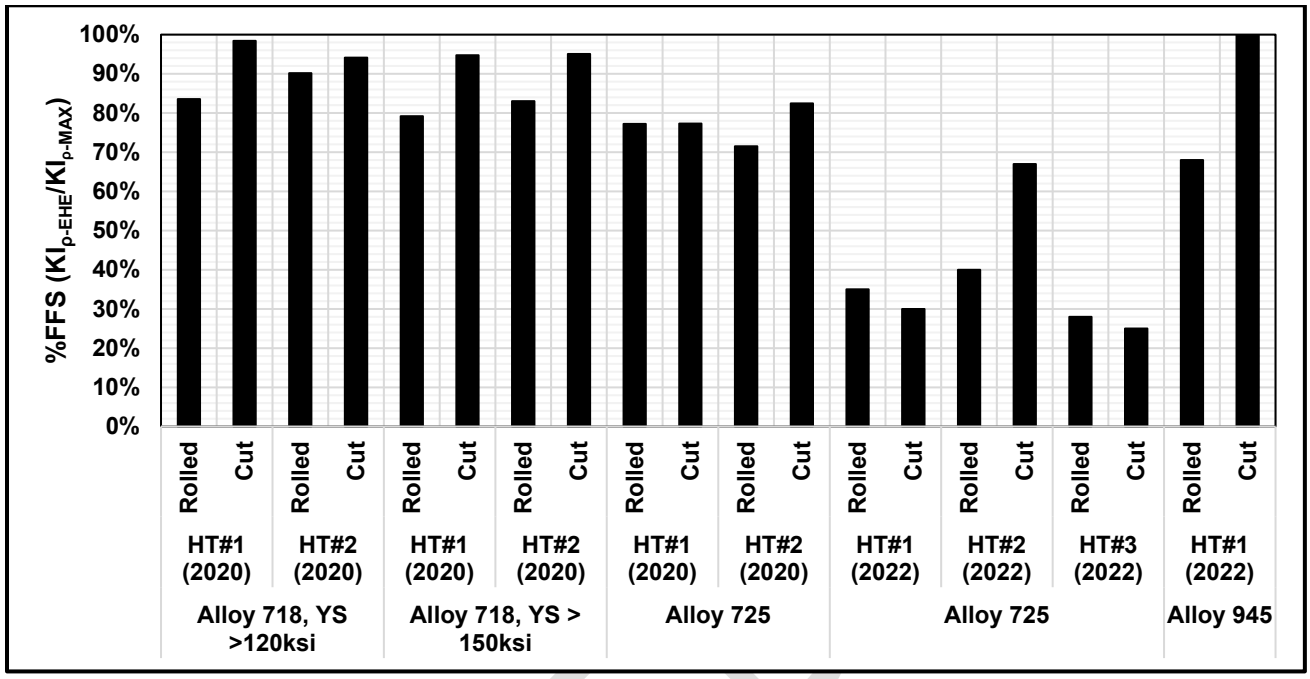

Figure 9-%FFS of alloys tested.

6.4 Consideration of Fracture Mechanics for HISC Susceptibility Assessment of Fasteners

6.4.1 The DTI Parameter

In addition to threshold stress intensity, the Damage Tolerance Index (DTI) and Hydrogen Susceptibility Ratio (Hsr) parameters of each thread type and for each grade were calculated. The DTI, or DTI as a function of KI_C, (i.e. from typical KI_C specimens, which is KI_C/UTS), provides a relative assessment of the critical defect size under a given stress intensity for the material. In general, this defect geometry is typically a controlled pre-crack used to determine KI_C from standard fracture toughness testing specimens per ASTM E399.

However, for the purposes of this testing program, the defect geometry is the natural cut or rolled thread root and must be represented differently. These novel fracture toughness specimens which utilize "thread-as-notch" defect geometry therefore result in a "KI_ρ" parameter; and the maximum stress intensity on a thread-as-notch specimen is then $KI_{\rho\text{-}MAX}$. This subsequently can be expressed in terms of DTI, called $DTI_{\rho\text{-}MAX}$, when represented as $KI_{\rho\text{-}MAX}$/UTS.

By extension, the critical defect (i.e. thread-as-notch geometry) which is loaded to the threshold stress intensity for onset of subcritical crack growth in a 3.5% NaCl solution with simulated CP becomes $DTI_{\rho\text{-}EHE}$ and represented by $KI_{\rho\text{-}EHE}$/UTS. Figure 10 shows the $DTI_{\rho\text{-}EHE}$ comparison between cut and rolled threads for all alloys tested. $DTI_{\rho\text{-}EHE}$ analysis of the bolts, revealed that despite having similar threshold stress intensities, cut thread specimens from alloy 945-120k showed a higher resistance to crack growth than 725-120k (2020); alloy 945-120k reached a DTI value maximum of 0.66 while alloy 725-120k (2020) reached a maximum DTI of 0.58. The calculated $DTI_{\rho\text{-}EHE}$ and Hsr parameters for the alloys tested are shown in Table 5. All values shown have used UTS in their calculation.

Table 5- The calculated DTI and Hsr parameters for all alloys with both cut and rolled threads.

Material Type	Heat ID	Thread Type	Hsr	$DTI_{\rho\text{-}EHE}$ ($\sqrt{in}$)
718-120k	1	Cut	1.86	0.58

		Rolled	1.64	0.58
	2	Cut	1.81	0.67
		Rolled	1.72	0.63
718-150k	1	Cut	2.01	0.74
		Rolled	1.73	0.62
	2	Cut	1.96	0.73
		Rolled	1.73	0.64
725-120k (2020)	1	Cut	1.52	0.56
		Rolled	1.46	0.53
	2	Cut	1.40	0.58
		Rolled	1.58	0.51
725-120k (2022)	1	Cut	0.61	0.21
		Rolled	0.73	0.25
	2	Cut	1.40	0.50
		Rolled	0.79	0.30
	3	Cut	0.48	0.18
		Rolled	0.55	0.20
945-120k	1	Cut	1.79	0.65
		Rolled	1.33	0.49

The empirical relationship between DTI using standard ASTM E399 KI_C specimens and $DTI_{\rho\text{-}MAX}$ using various thread-as-notch specimens is still not fully understood, however evidence suggests they have a proportional relationship. Further study is necessary to fully quantify this relationship.

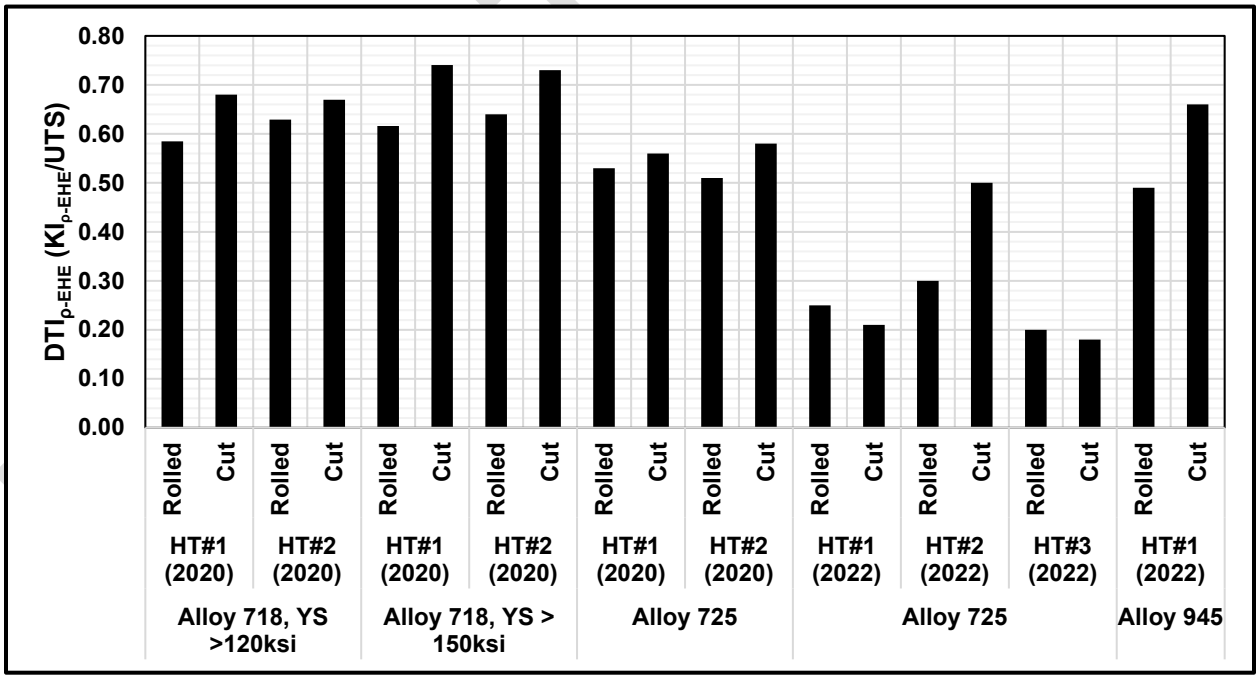

Figure 10- Comparison of the $DTI_{\rho\text{-}EHE}$ parameter for each alloy with both cut and rolled threads.

The $DTI_{\rho\text{-}EHE}$ parameter (also referred to as the Flaw Tolerance Ratio) is a useful metric to quantify the sensitivity of a material to defects (i.e. the material's resistance to fracture); or in the case of this test program, the material's resistance to fracture

in a CP environment with a formed thread. Originally used for the U.S. Navy's Fracture Toughness Review Process (FTRP) and Materials Selection Process (MSP), the DTI is used as a normalized metric that can be easily obtained in laboratory conditions to quantify the behavior of materials in the presence of defects[3]. A material with DTI ≥ 1 indicates the fracture toughness meets or exceeds the material's tensile strength, which implies the material would begin yielding well before the onset of crack growth. As an example, high-ratio DTI values have been used in the U.S Navy's FTRP-MSP where a minimum DTI of 1.15 is required to establish a safety factor. A material with DTI < 1 can theoretically fracture under purely elastic conditions. However, it is recommended to subsequently determine the Hsr parameter for a material where DTI < 1 to assess if there is potential susceptibility to HISC within the presumed brittle fracture region.

6.4.2 The Hsr Parameter

The Hydrogen Susceptibility Ratio, Hsr, parameter provides insight into the magnitude of effect a specific threaded geometry, or surface geometry, has on the hydrogen embrittlement susceptibility of the given material. The Hsr parameter for specimens in bending is similar to the Notch Strength Ratio (NSR) for specimens in uniaxial tension[4]. Hsr is calculated by dividing the threshold stress for onset of crack growth of the test specimen by the material's UTS ($\sigma_{Threshold}$/UTS). In this testing program, $\sigma_{Threshold}$ was the stress at which onset of crack growth of a thread-as-notch specimen in a 3.5% NaCl solution with simulated CP was observed and the UTS was based on the values reported in the MTRs and shown in Table 1. Figure 11 shows the Hsr comparison between cut and rolled threads for all alloys tested.

An ideal notched low alloy steel round bar specimen pulled in tension at loading rates per ASTM E8 will typically rupture at a maximum NSR of 1.5; however, it is expected that the ratio decreases as material hardness and tensile strength increase[5,6]. In comparison, when loaded in bending, ideal notched specimens can reach a limit of Hsr=2 before specimens experience net section yielding[7]. In notched tensile tests, an NSR > 1 indicates that the specimen is likely to experience ductile failure rather than brittle failure. Similarly, a fastener with a measured Hsr value ≥ 1 will theoretically experience yielding before HISC failure due to EHE when in service. In practice, an Hsr minimum criteria of 1.2 for bolts in tension can be used to provide a margin of safety in various applications[8].

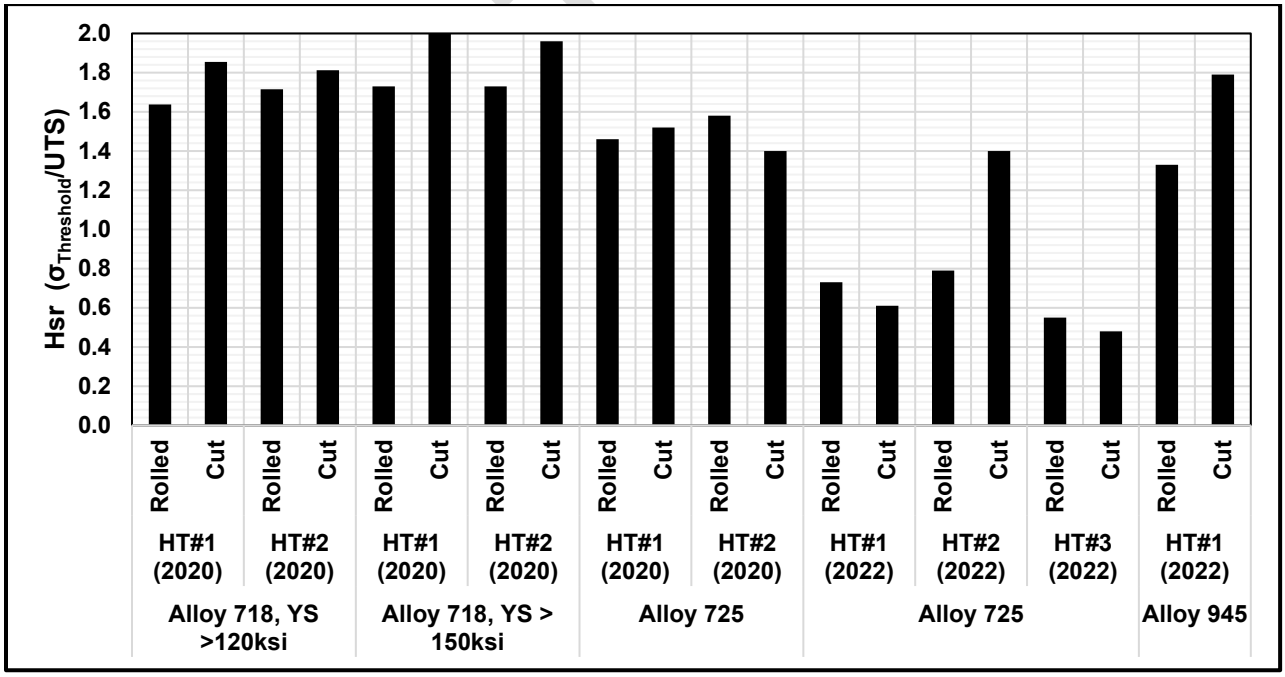

Figure 11- Comparison of the Hsr parameter for each alloy with both cut and rolled threads.

Hsr measurements from notched square-bar specimens tested in bend validated initial observations. Specimens with cut threads from alloy 718-150k Heat 1 and 718-150k Heat 2 had Hsr values of 2.01 and 1.96, respectively, evidence that despite

being exposed to a 3.5% NaCl solution and simulated CP during the ASTM F1624 ISL testing, these specimens essentially reached their theoretical bending load limit. This means that hydrogen produced from the CP had very little, if any, effect on the specimens. Alloy 725-120k (2022) was found to have an exceptionally low Hsr when tested in bend. All alloy 725-120k (2022) specimens, except for cut threads from 725-120k (2022) Heat 2, had an Hsr < 1.0 which is an indicator of increased risk of brittle failure during service if exposed to conditions like those tested.

NOTE: See Annex A and Annex B for additional detail on fracture mechanics, Hsr and DTI equation derivations, and example calculations.

6.5 Observations on Alloy 725-120k

6.5.1 General

Due to the disparate results for alloy 725-120k (2020) and alloy 725-120k (2022), additional metallurgical and chemical composition overcheck testing were performed to assess if there were any microstructural differences between both heats which might explain the disparate behavior in testing. A sample of material from alloy 725-120k (2020) Heat 1 and alloy 725-120k (2022) Heat 1, both with rolled threads, were investigated. All samples were hot mounted, polished, and etched (Etchant #22a per ASTM E407) to reveal the microstructures.

6.5.2 Alloy 725-120k Microstructural Observations

Alloy 725-120k (2020) in Figure 12 and alloy 725-120k (2022) in Figure 13 both show similar microstructural deformation from cold work due to roll threading operations. The threads are indicative of a heavily work hardened area, where the darker areas are evidence of high dislocation slip band density. Similar microstructure morphology can be seen at the thread roots as well; however, the cross-sectional area is smaller and suggests a lower depth of work hardening. Immediately under the threads and thread root, slip bands and twinning are observed in a subsurface secondary cold work zone. Beyond the subsurface zone is material unaffected by the thread rolling process, where the microstructure observed is analogous to the microstructure from the original MTR. While thread microstructure examination was performed on alloy 725-120k, the observed microstructure for rolled threads is still indicative of what would be present in all PHNAs tested with rolled threads.

NOTE The inset boxed areas at bottom of Figure 12 and Figure 13 are the microstructures observed in the top and bottom, respectively, of Figure 14.

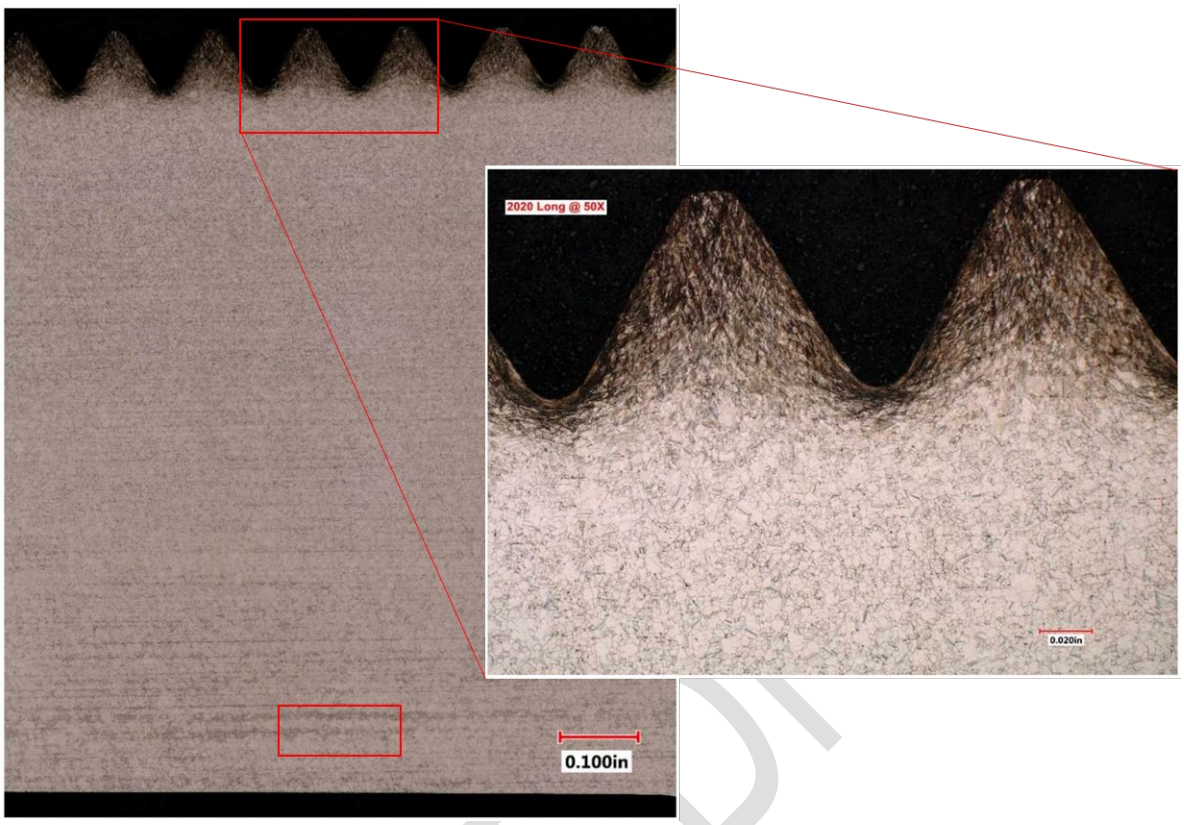

Figure 12-Cross-section microstructure of alloy 725-120k (2020), including magnification of rolled threads.

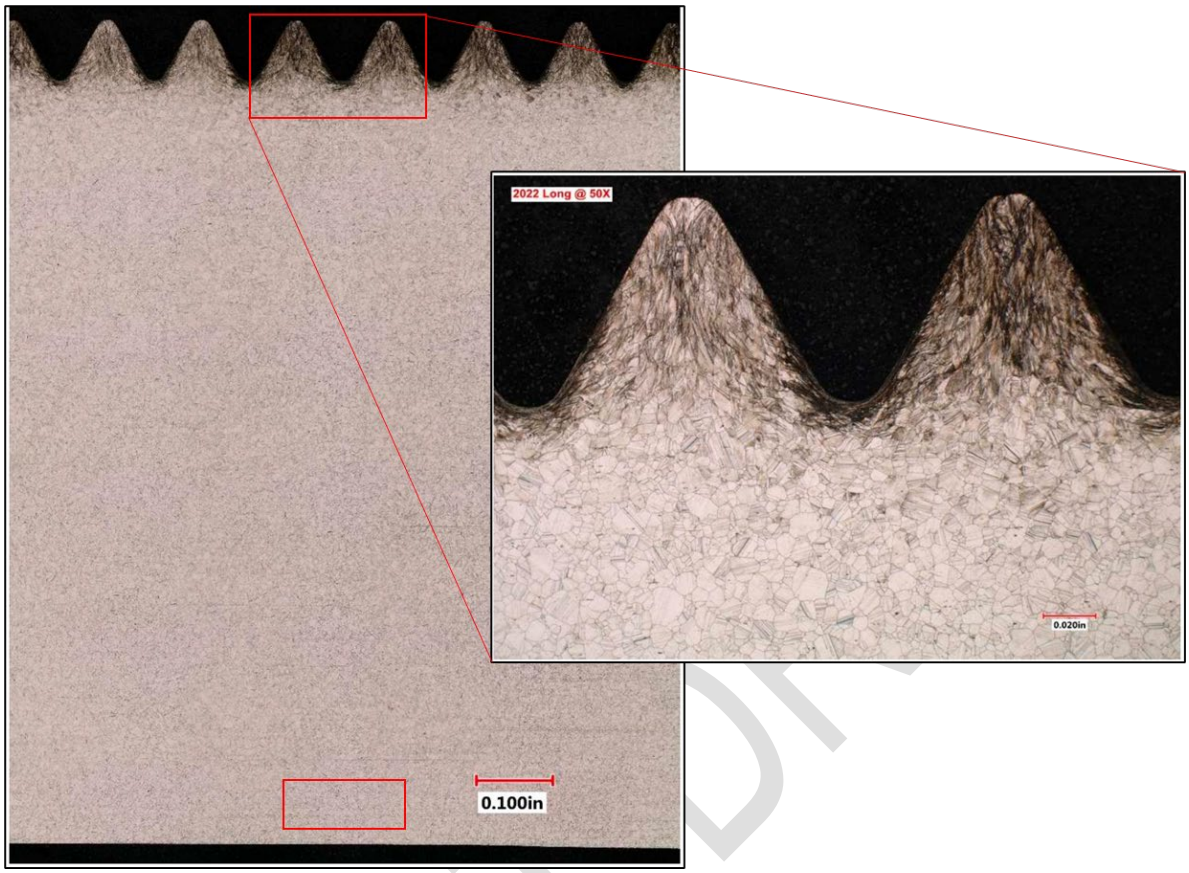

Figure 13- Cross-section microstructure of alloy 725-120k (2022), including magnification of rolled threads.

The microstructure of alloy 725-120k (2020), except for the areas affected by cold work from roll threading operations, exhibits a relatively equiaxed microstructure. However, the center of the bar exhibits a duplex topological structure with a mix of both very fine and large grains, and high levels of precipitates present. The 725-120k (2020) microstructure was duplex, wide-range, ASTM No. 5.5, with a range of ASTM No. 2 to ASTM No. 8.5. Since the original MTRs for all materials were stated in compliance with API 6ACRA 1st edition, it is likely the microstructure observed is anomalous to the heat and it is plausible to be an isolated instance within the original bar processed for this testing program. However, as observed, the duplex topological structure would not meet the microstructure requirements of API 6ACRA 1st edition. In comparison, the microstructure of alloy 725-120k (2022) exhibits a uniform, equiaxed microstructure with a grain size of ASTM No. 3.5, and with very few precipitates present throughout the cross-section. Figure 14 shows a comparison of both microstructures at the center of the threaded bar.

Because grain boundaries and precipitates can act as trapping sites for hydrogen, these microstructural variations can have a significant impact on HE susceptibility. However, the duplex topological structure in alloy 725-120k (2020) was observed at center of the bar and therefore would neither be affected by the roll threading operations nor be immediately exposed to the test environment and thereby impact the HE susceptibility of the specimens tested. Due to the microstructures observed at the stated locations and the similarities of thread microstructure, no correlation to the disparate testing results between 725-120k (2020) and 725-120k (2022) could be determined by microstructure alone.

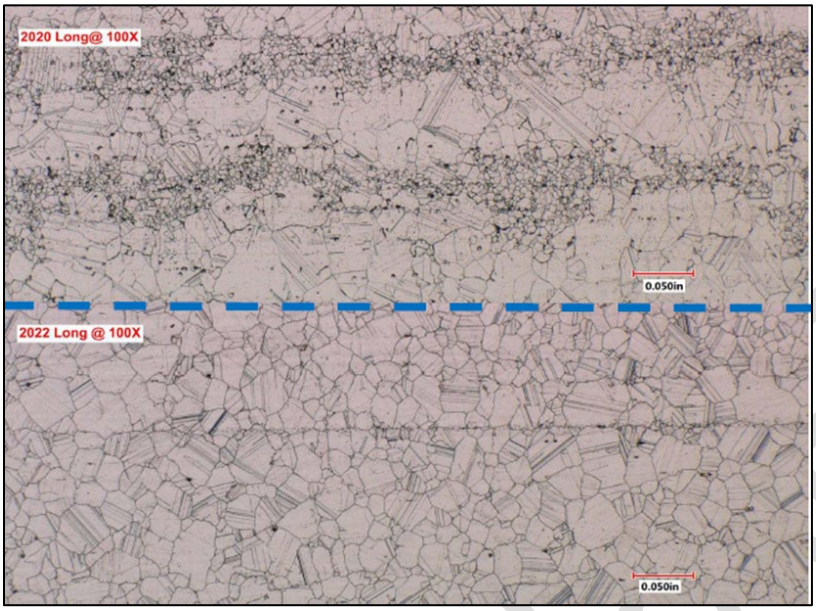

Figure 14-Comparison of microstructure at center of threaded bar (T/2 location) for alloy 725-120k (2020) (top) and alloy 725-120k (2022) (bottom).

6.5.3 Alloy 725-120k Chemical Composition Observations

The chemical composition of alloy 725-120k (2020) and alloy 725-120k (2022) were evaluated and the results are shown in Table 5. The MTRs include elements determined by optical emission spectroscopy (OES) and x-ray fluorescence. The as-tested data was evaluated using a combination of inductively coupled plasma (ICP) and combustion analysis.

Both samples met the compositional requirements of API 6ACRA. The alloy 725-120k (2020) sample showed much higher $KI_{\rho\text{-}EHE}$ results, despite an observed marginally banded microstructure as compared to the alloy 725-120k (2022) sample. Upon review, there were slight differences in the averaged Titanium (Ti) content between alloy 725-120k (2020) at 1.26 wt% and alloy 725-120k (2022) at 1.53 wt%. The role of Titanium (Ti) in HISC susceptibility of alloy 725 is being explored in other industry testing[9].

Table 5-Chemical composition comparisons of 725-120k (2020) and 725-120k (2022)

Element	725-120k (2020)		725-120k (2022)	
	As-Tested	MTR	As-Tested	MTR
C	0.02	0.014	0.01	0.007
Ca	-	0.001	-	0.0003
B	-	0.0028	-	0.001
Mn	0.04	0.05	0.03	0.04
Si	0.07	0.06	0.06	0.05
P	0.01	0.003	0.01	0.005
S	<0.005[a]	0.0005	<0.005[a]	0.0005
Cr	20.5	21.0	21	21.78
Ni	58.4	57.6	58.6	57.39
Nb	3.33	3.40	3.35	3.45
Ti	1.28	1.24	1.44	1.51
Al	0.22	0.19	0.29	0.29
Mo	8.1	8.01	8.12	8.14
Fe	Balance	8.13	Balance	7.22

FOOTNOTE

[a] Value listed is the lowest resolvable limit by OES testing equipment; actual value lower is than what is shown.

7 Conclusions and Recommendations

7.1 Hardness Testing Conclusions

From the hardness testing conducted and observations of the resulting data, the following conclusions can be made.

- Thread rolling results in an increased hardness within the threads due to work hardening.
- Cut threading shows a little-to-no increase in hardness.
- The depth of hardness increase into the base metal is dependent on the threading process utilized and the starting base metal hardness.

7.2 Fracture Toughness and ISL Conclusions

From the fracture toughness testing conducted, the ISL testing, and observations of the resulting data, the following conclusions can be made.

- The effect of thread rolling appears to show higher sensitivity to EHE from CP.
- Alloy 718-150k was found to have the highest $KI_{p\text{-}MAX}$ and $KI_{p\text{-}EHE}$ values, indicating the best performance using a thread-as-notch specimen geometry in the tested environment.
- Specimens with cut threads from alloy 718-150k and alloy 945-120k were found to show very little susceptibility to EHE. However, testing of additional heats of alloy 945-120k are recommended to determine if results are indicative of general performance of the material.
- Alloy 725 appears to show the most susceptibility of all materials tested to EHE due to CP.

- Alloy 725-120k (2022) was found to have a much lower threshold for EHE than alloy 725-120k (2020). Differences in microstructure and chemical composition were found that may account for this phenomenon, however, could not be determined through the scope of testing performed. Further research into this area is recommended.
- Alloy 718-150k with cut threads attained an Hsr = 2.01 which indicates specimens had reached the theoretical bending load limit, indicative of negligible susceptibility to EHE.
- The DTI and Hsr parameters are useful to correlate various fracture mechanics concepts together. However, further study of the relationship between KI_C (ASTM E399) to $KI_{\rho\text{-}MAX}$ (thread-as-notch) is recommended for PHNAs to develop this specific correlation factor.
- The DTI and Hsr parameters can aid in selection of bolting sizes and types which can minimize susceptibility of PHNAs to hydrogen embrittlement by CP. Thread Fracture Susceptibility (TFS) diagrams may be used to graphically represent the DTI-Hsr-bolt geometry correlation.
- The calculated Hsr slope of any TFS diagram is dependent on the thread type used, since its parameters depend on the major and minor thread diameters.
- The calculated Hsr slope, based on Equation A.14 and as seen in Figure B.2, will trend in the direction of a positive slope. This indicates that smaller bolting sizes have a larger DTI range (i.e. load tolerance) which can help avoid the brittle fracture region.
- The DTI and Hsr parameters can provide additional bolting design parameters to aid in application performance and quality control.

Annex A
(informative)

Summary of Fracture Mechanics and Background of DTI and Hsr Equations

A.1 Basics of KI_C and Notch Effect Fracture Mechanics

A.1.1 Loading Modes

While typical tensile properties are sufficient to describe materials in the majority of use cases, materials can exhibit unexpected behaviors in the presence of notches and sharp cracks. As a smooth round bar is pulled in tension past the material yield strength, an observer will often see a section of the specimen begin to neck due to a triaxial state of stress. In other words, as a test coupon begins to deform plastically, the material will begin to stretch in a direction parallel to the direction of the applied load. However, since the conservation of volume applies to the plastic deformation process, the coupon will also attempt to contract laterally. Because the bulk of the material in the un-necked region is experiencing a lower true stress than the material in the necked region, it adds constraint to the material at the root of the necked area[10]. Similarly, when a specimen or part is intentionally notched, the notch acts to constrain the plastic deformation at the root of the notch (i.e., notched round bars and thread roots in bolts). The deeper the notch the greater the plastic constraint at the root of the notch, and thus the higher the applied stress necessary to deform the sample or part. In general, highly ductile materials will see an increase in the net section stress required to rupture as notch depth is increased (notch strengthening) while brittle materials will see a decrease in net section stress as the notch depth is increased (notch weakening).

The toughness of the material is defined as the energy absorbed before fracture and can be quantified as the area under the stress-strain curve. With notched specimens, there are three defined basic modes of loading with regards to fracture toughness[11]:

- Mode I: Opening/Tensile
- Mode II: Sliding/In-Plane Shear
- Mode III: Tearing/Out-Of-Plane Shear

This Annex will focus solely on Mode I, the tensile mode where the crack is pulled apart directly, because Mode I is the most applicable to situations involving bolts pulled in tension.

A.1.2 Stress Intensity

The Stress Intensity Factor, K, describes the magnitude of the stress field at the tip of a crack and is the typical variable used to describe the fracture toughness of a material. The material property, "KI_C", is the stress intensity (K) of a material in Mode I (I) loading at a critical load where fracture occurs under plane strain conditions (subscript C) and is the most common fracture toughness metric referenced. The stress intensity is calculated as a function of stress and the crack size of a part or specimen as shown below. Other factors also play a role in stress intensity calculations such as the load orientation and the overall part/specimen geometry. The stress intensity factor can be calculated as follows:

$$K = Y\sigma\sqrt{\pi a} \tag{A.1}$$

where,

- Y is a geometry correction factor that considers part geometry and load orientation (see Equation A.2)
- σ is the gross stress on a part or specimen, typically expressed in psi or ksi (kPa or MPa)
- a is either the critical edge crack length (external crack-like flaw) or half the crack length (internal crack-like flaw), expressed in in. (mm)

For a single-edge notched specimen loaded in 4-point bend (SEN(B)), the geometry factor, Y, is a function of the crack depth and the specimen width, f(a/W), that can be calculated with the following empirical equation using the dimensions expressed in Figure A.1[12]:

$$Y = f\left(\frac{a}{W}\right) = 1.22 - 1.40\left(\frac{a}{W}\right) + 7.33\left(\frac{a}{W}\right)^2 - 13.08\left(\frac{a}{W}\right)^3 + 14.0\left(\frac{a}{W}\right)^4 \quad \text{(A.2)}$$

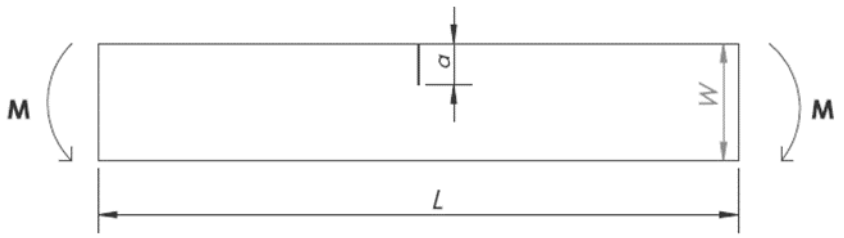

Figure A.1- "*a*" and "W" dimensions for a typical SEN(B) specimen.

As discussed previously, when a specimen is stressed in tension past a point, specifically its yield strength (σ_Y), the material will begin to deform plastically in a direction that is parallel to the crack (normal to the direction of applied stress). If a sample is of sufficient thickness, however, large stresses can be generated in the z-direction (parallel to crack) that restrict the plastic deformation in this direction. This phenomenon is analogous how a notch at the root of a crack can also restrict the plastic deformation at the crack tip. Accordingly, the fracture toughness will depend on specimen thickness, generally decreasing as the specimen thickness increases. Once the thickness reaches a critical dimension sufficient to have plane-strain conditions at the crack tip, the KI_C can be determined and will serve as the lower limit of the material's fracture toughness. Some guidelines are available in ASTM E399 to determine whether a test coupon is of sufficient thickness for plane-strain conditions to be present. Generally, the minimum thickness for plane-strain conditions, BI_C, can be determined from the following equation[13]:

$$BI_C = 2.5\left(\frac{KI_C}{\sigma_Y}\right)^2 \quad \text{(A.3)}$$

A.2 The DTI Equation and Focus Principles

The Damage Tolerance Index (DTI) is a metric to describe the critical flaw geometry of a given part. Because DTI is defined as the quotient of the critical stress intensity and a material's YS or UTS, the standard stress intensity equation per Equation A.1 can be rewritten as follows to relate DTI to critical flaw sizes (i.e. flaw tolerance):

$$K = Y\sigma\sqrt{\pi \cdot \text{crack depth}} \quad \text{(A.4)}$$

Since KI_C is the critical fracture toughness of a material in Mode I uniaxial tension under plane strain conditions at the maximum Mode I stress (σ_{MAX}), we can further rewrite the equation to:

$$KI_C = Y\sigma_{MAX}\sqrt{\pi \cdot \text{crack depth}} \quad \text{(A.5)}$$

Further, because designing to a material's yield strength (σ_Y) is a common engineering design criterion rather than designing to the maximum limit, at the yield strength the resulting maximum design stress intensity ($K_{D\text{-}MAX}$) can be found by the following equation.

$$K_{D-MAX} = Y\sigma_Y\sqrt{\pi \cdot \text{crack depth}} \quad \text{(A.6)}$$

NOTE 1 The maximum design stress intensity is irrespective of loading Mode to maintain conservatism.

NOTE 2 It is also common to substitute a material's yield strength with a different specific design strength value, such as using a safety factor or other design strength requirement, to maintain conservatism.

The geometry parameters of the part can be isolated by dividing both sides of Equation A.6 by σ_Y as shown below:

$$\frac{K_{D-MAX}}{\sigma_Y} = Y\sqrt{\pi \cdot \text{crack depth}} \quad \text{(A.7)}$$

Since DTI is defined as the ratio of stress intensity to a given stress (in this case, a design yield strength), Equation A.7 can be rewritten to show the relationship between DTI, the stress intensity ratio, geometry, and the critical flaw size for a given part:

$$DTI = \frac{K_{D-MAX}}{\sigma_Y} = Y\sqrt{\pi \cdot \text{crack depth}} \quad \text{(A.8)}$$

A.3 Expansion Principles for KI_C and DTI

A.3.1 General

As explained, under plane-strain conditions the critical stress intensity at which brittle failure will occur is a material property known as KI_C. Dividing this value by the material's yield strength will provide the maximum DTI of the material under plane-strain conditions, which can also be expressed as $DTI_{\sigma Y\text{-}MAX}$. By extension, dividing by the material's tensile strength would be more conservative and can be expressed as $DTI_{\sigma T\text{-}MAX}$.

As shown above, the DTI is a function of the geometry and the critical flaw size for a given material. Because KI_C can be measured in a laboratory setting using representative test coupons, the DTI of the material is an additional metric that can be calculated to relate the performance of laboratory coupons to full-sized parts in service.

Similar principles can be applied to other stress intensity metrics. For example, if $KI_{C\text{-}EHE}$ represents the critical stress intensity at which subcritical crack growth due to external hydrogen embrittlement (e.g., HISC) will occur in a specific environment, the DTI_{EHE} can be measured using the same laboratory specimens exposed to environmental conditions similar to what the final parts will experience while in service. DTI_{EHE} can then be used as a metric of the critical flaw size for a material when exposed to a given environmental condition.

A.3.2 Fracture Mechanics Applied to Fasteners

The methods described can also be used to predict the behavior of full-sized fasteners in service conditions from the results of simple laboratory tests on representative coupons. Rather than a sharp crack, the individual thread features are modeled as a notch in the material which act to concentrate stress near the thread root. Because of this, we can modify Equation A.1 again to calculate the relative stress intensity at the root of the threads, KI_ρ, by substituting the crack depth with the thread depth as shown below:

$$KI_\rho = Y\sigma\sqrt{\pi \cdot \text{thread depth}} \quad \text{(A.9)}$$

Because a thread root will typically be considerably blunter than a sharp fatigue crack, the variable "ρ" (Greek "rho") is used to denote that the stress intensity values are representative of a test coupon which utilizes a thread root, rather than a sharp crack feature. By relating fracture mechanics concepts to thread features, a broader range of methods can be used to analyze and predict behavior of fasteners. Both sides of the equation can subsequently be divided by the material's yield or tensile strength to determine the DTI_ρ, which can be used to relate the performance of small-scale laboratory specimens to full-sized bolts in service.

A.4 The Hsr Equation and Focus Principles

The Hydrogen Susceptibility Ratio, Hsr, is defined as the threshold stress for the onset of subcritical crack growth due to HISC ($\sigma_{HISC\ Threshold}$) divided by the material's YS (σ_Y) or UTS (σ_{UTS}). When the Hsr > 1, the applied stress on the part which begins the onset of subcritical crack growth, exceeds the material's YS or UTS. As a result, some amount of plastic flow will be present at the time of crack growth. While the material's YS is typically used as a design parameter, the UTS is a more conservative metric to ensure that there is sufficient plasticity around the notch. The Hsr ratio can be written as the following equation:

$$Hsr = \frac{\sigma_{HISC\ Threshold}}{\sigma_Y \text{ or } \sigma_{UTS}} \tag{A.10}$$

For the example of threaded fasteners, the HISC threshold stress is the maximum stress on a specimen which uses a thread as the notch and exposed to simulated CP. Hsr can then be rewritten as:

$$Hsr = \frac{\sigma_{\rho-EHE}}{\sigma_Y \text{ or } \sigma_{UTS}} \tag{A.11}$$

Equation A.9 can now be rewritten in terms of threaded specimens which are exposed to simulated CP:

$$KI_{\rho-EHE} = Y\sigma_{\rho-EHE}\sqrt{\pi \cdot \text{thread depth}} \tag{A.12}$$

By measuring $KI_{\rho\text{-}EHE}$, both $DTI_{\rho\text{-}EHE}$ and Hsr can be calculated by normalizing the equation against the material's YS or UTS as shown below:

$$\frac{KI_{\rho-EHE}}{\sigma_Y \text{ or } \sigma_{UTS}} = \frac{Y\sigma_{\rho-EHE}\sqrt{\pi \cdot \text{thread depth}}}{\sigma_Y \text{ or } \sigma_{UTS}} \tag{A.13}$$

Since Hsr is the ratio of threshold stress for HISC versus the material YS or UTS, and $DTI_{\rho\text{-}EHE}$ is the ratio of threshold stress intensity versus the material YS or UTS for onset of crack growth in a thread while under CP, the equation can be rewritten as follows:

$$DTI_{\rho-EHE} = Hsr \cdot Y\sqrt{\pi} \cdot \sqrt{\text{thread depth}} \tag{A.14}$$

NOTE: This equation is graphically represented in Figure B.2.

A.5 Development of the DTI and Hsr Parameters

Although not referred to by name, the concept of using a DTI-like metric to relate fracture toughness data to a critical flaw was first introduced in 1964 when it was used to establish non-destructive acceptance criteria for materials used to make high pressure tanks. As presented in ASTM STP 381, notched round bar specimens and specimens with elliptical surface flaws or internal flaws were originally used to determine the fracture toughness properties of different materials as candidates for use in pressure vessels. To normalize for the influence of material strength levels, the fracture toughness was divided by the tensile strength, and the index was squared, i.e., $(KI_C/UTS)^2$, to maintain standard units. This metric was then used to compare the resistance of the material candidates to flaws of different sizes[2]. These principles were also used to create graphical representations of predicted flaw sizes versus DTI[14,15].

These ideas were later adopted in the early 2000s into the U.S. Navy's NAVSEA Fracture Toughness Review Process (FTRP) and Materials Selection Process (MSP)[3] as the coined terms "DTI" and "Hsr", for the determination of acceptability

of flawed components for use in pressure vessels to ensure a “leak before burst” failure mode, including when CP is present. While originally designed with pressure vessels in mind, the metric can prove extremely useful in analyzing the behavior of fasteners, as evidenced in the derived equations, to assess for a ductile failure mechanism even under EHE conditions.

Annex B
(informative)

Practical Application and Example Calculations of DTI and Hsr

B.1 Application of DTI and Hsr for Practical Assessment

The DTI serves as a metric that can be calculated based on variables independent of part geometry, meaning information gathered from a simple laboratory test can be extrapolated to different applications. If a given material-geometry combination is found to have a DTI ≥ 1, this eliminates (under perfect conditions) the propensity for fracture to occur under purely elastic stresses[3]. Where DTI < 1, further assessment would be necessary to determine material acceptance. Thus, a more accurate representation of performance uses both DTI and Hsr for threaded fasteners when DTI < 1. See example calculations in B.2.

The use of fracture mechanics equations to characterize the performance of full-sized bolts in service conditions via laboratory testing was validated during a failure investigation for the for the California Department of Transportation. ASTM A354 Grade BD threaded, double-ended rods with diameters larger than 2.5 in. (63.5 mm) were found to have prematurely fractured during construction of the San Francisco-Oakland Bay Bridge in ca. 2013[16]. Tests V and VI of the laboratory testing program detailed in Reference [16] outline the processes used to measure the threshold stress intensity for the onset of hydrogen induced crack growth from sub-sized threaded test coupons pulled from the outer diameter of the rods. The threshold stress intensity (KI_ρ) was then used to extrapolate the breaking load of the full-sized rods in service conditions. The laboratory testing was later validated by testing of full-size ASTM A354 threaded, double-ended rods in Test VI where a nearly 90% correlation between Test V and VI results was achieved.

From Test V, KI_ρ measurements taken from the sub-sized test coupons proved to be extremely beneficial in predicting the failure points of full-sized rods in service conditions. With the validation of the relationship of the fracture mechanics of sub-sized coupons and full-sized bolts established, a minimum criterion for DTI was then established for a given bolt diameter to ensure that future bolts will experience yield before brittle failure due to EHE.

B.2 Example Calculations

With respect to the bolts tested in this program, the DTI can be a very useful comparison tool to determine which alloys would produce bolts that are more likely to yield before brittle fracture due to EHE (e.g., HISC). For example, if $DTI_{\rho\text{-}EHE}$ is known for a given material, and a minimum Hsr value is defined for minimum acceptance, then it is possible to calculate a maximum bolt diameter allowable to ensure ductile failure, which is the geometry factor in the stress intensity equation. Alternatively, if the bolt geometry necessary for a certain application is known and the criteria for Hsr is again defined, the minimum $DTI_{\rho\text{-}EHE}$ can be calculated and used as a factor for material selection. $DTI_{\rho\text{-}EHE}$ calculation can easily be obtained from representative coupons tested in laboratory settings. The following example calculations outline three scenarios in which DTI and Hsr can be used to expand upon the previously measured laboratory data.

EXAMPLE 1 Where DTI < 1

A 1.5” (38.1 mm) diameter alloy 718 (UNS N07718) bolt with UNR series threads is loaded under pure tension and exposed to CP. Laboratory ASTM F1624 testing indicates $KI_{\rho\text{-}EHE}$ of 132.5 ksi•√in for threaded specimens. The alloy 718 material has a measured yield strength of 154 ksi (1,061.8 MPa) and a measured tensile strength of 181 ksi (1,248.0 MPa). The thread depth for UNR threads per ASME B1.1 is 0.08395 in. (2.1 mm) based on a major diameter (D) of 1.5 in. (38.1 mm) and a minor diameter (d) of 1.3321 in. (33.8 mm).

$DTI_{\rho\text{-}EHE}$ can be calculated as follows:

$$DTI_{\rho-EHE} = \frac{KI_{\rho-EHE}}{\sigma_Y} \quad \text{(B.1)}$$

$$DTI_{\rho-EHE} = \frac{132.5\ \text{ksi}\bullet\sqrt{\text{in}}}{154\ ksi} \quad \text{(B.2)}$$

$$DTI_{\rho-EHE} = 0.860\ \sqrt{\text{in}} \quad \text{(B.3)}$$

Since DTI < 1, there exists possibility of brittle fracture by HISC at stresses below the yield stress. In this case, Hsr should be determined for the full-sized fastener in tension from the data of a sub-sized specimen by laboratory testing. To relate the square notched specimen from ASTM F1624 testing in bending to the round specimen from ASTM E8 testing in tension, Equation A.14 can be used, which is restated below:

$$DTI_{\rho-EHE} = Hsr \cdot Y\sqrt{\pi} \cdot \sqrt{\text{thread depth}} \quad \text{(B.4)}$$

For a notched round bar pulled in tension, the geometry factor, Y can be found using the following equation[12] in conjunction with the thread depth based on the ASME B1.1 major and minor diameters for a 1.5" (38.1 mm) fastener with UNR threads:

$$Y = f\left(\frac{d}{D}\right) = \frac{1}{2}\sqrt{\left(\frac{d}{D}\right)} \cdot \left(1 + \frac{1}{2}\left(\frac{d}{D}\right) + \frac{3}{8}\left(\frac{d}{D}\right)^2 - 0.363\left(\frac{d}{D}\right)^3 + 0.731\left(\frac{d}{D}\right)^4\right) \quad \text{(B.5)}$$

$$Y = f\left(\frac{d}{D}\right) = 0.8612 \quad \text{(B.6)}$$

Hsr can then be calculated as follows:

$$0.86\sqrt{in} = Hsr \cdot 0.8612\sqrt{\pi} \cdot \sqrt{0.08395\ in} \quad \text{(B.7)}$$

$$Hsr = 1.83 \quad \text{(B.8)}$$

Since Hsr > 1, the fastener will experience yielding prior to failure due to HISC.

EXAMPLE 2 Where DTI > 1

A 1.5 in. (38.1 mm) diameter alloy 945 (UNS N09945) bolt with UNR series threads is loaded under pure tension in air in a dry environment. The bolts are not treated with any embrittling processes, so there is no residual hydrogen present within the material. Laboratory testing indicates a $KI_{\rho\text{-max}}$ of 140.5 ksi•√in using threaded specimens. The alloy 945 material has a measured yield strength of 130 ksi (896.3 MPa) and a measured tensile strength of 165 ksi (1,137.6 MPa). The thread depth for UNR threads per ASME B1.1 is 0.08395 in. (2.1 mm) based on a major diameter (D) of 1.5 in. (38.1 mm) and a minor diameter (d) of 1.3321 in. (33.8 mm). The design does not expect the bolts to see high loads and therefore the material's yield strength is used to calculate DTI.

$DTI_{\rho\text{-max}}$ can be calculated as follows:

$$DTI_{\rho-MAX} = \frac{KI_{\rho-MAX}}{\sigma_Y} \quad \text{(B.9)}$$

$$DTI_{\rho-MAX} = \frac{140.5\ \text{ksi}\bullet\sqrt{\text{in}}}{130.0\ ksi} \quad \text{(B.10)}$$

$$DTI_{\rho-MAX} = 1.08\ \sqrt{\text{in}} \quad \text{(B.11)}$$

Since the $DTI_{\rho\text{-MAX}}$ > 1, the probability of the bolts experiencing brittle failure in purely elastic conditions when loaded in air is low.

To ensure the results are conservative, the material's tensile strength could be used to calculate DTI. In this example, the resulting DTI would be less than 1; therefore, additional analysis (shown in Example 1) would be necessary to assess suitability in the specific service conditions.

EXAMPLE 3 Determine optimal fastener diameter with set DTI and Hsr design criteria

Alloy 718 is selected as a candidate material for bolting in subsea conditions under CP. A designer wants to make a 1.5" (38.1 mm) diameter UNS N07718 bolt with series 16-UNR threads from the selected material and needs to ensure that it will yield before failing due to HISC. Laboratory testing of the material finds a $KI_{\rho\text{-}EHE}$ of 80.4ksi√in, a YS of 125.6 ksi (866.0 MPa), and a UTS of 178.7 ksi (1,232.1 MPa). The designer uses the both UTS to calculate $DTI_{\rho\text{-}EHE}$ to ensure the results are the most conservative:

$$DTI_{\rho-EHE} = \frac{KI_{\rho-EHE}}{\sigma_{UTS}} \quad \text{(B.12)}$$

$$DTI_{\rho-EHE} = \frac{80.4\ \text{ksi}\bullet\sqrt{\text{in}}}{178.7\ ksi} \quad \text{(B.13)}$$

$$DTI_{\rho-EHE} = 0.45\ \sqrt{\text{in}} \quad \text{(B.14)}$$

As described previously, when DTI < 1, secondary calculations for Hsr should be performed to determine the possibility of brittle fracture by HISC at stresses below the yield stress.

As shown in Equation A.13, if both sides are divided by either the YS or UTS, the stress intensity equation can be rewritten as follows:

$$DTI_{\rho-EHE} = Hsr \cdot Y\sqrt{\pi} \cdot \sqrt{Thread\ Depth} \quad \text{(B.15)}$$

Where Y is a geometry factor calculated as a function of the ratio of the minimum and maximum thread diameter. For the case of a notched round bar pulled in tension, i.e. a threaded bolt, the function is represented as the following:

$$Y = \frac{1}{2}\sqrt{\left(\frac{d}{D}\right)} \cdot \left(1 + \frac{1}{2}\left(\frac{d}{D}\right) + \frac{3}{8}\left(\frac{d}{D}\right)^2 - 0.363\left(\frac{d}{D}\right)^3 + 0.731\left(\frac{d}{D}\right)^4\right) \quad \text{(B.16)}$$

If an Hsr of 1.2, based on DTI calculations using UTS, is used as a minimum level to denote ductile behavior by notch strengthening in the bolt (i.e. notched round bar) the DTI equation can be rewritten as a function of the major and minor thread diameter.

NOTE The Hsr value selected in this example is for instructional purposes only.

$$DTI_{\rho-EHE} = 1.2 \cdot Y\sqrt{\pi} \cdot \sqrt{\frac{D-d}{2}} \quad \text{(B.17)}$$

Since the minor diameter is determined from the major diameter in most cases, the equation can be solved using known values of *D* and *d* to determine the minimum $DTI_{\rho\text{-}EHE}$ needed to for a bolt of each given diameter to meet a minimum criterion of Hsr ≥ 1.2. In the case of 12-UNR bolts, a Thread Fracture Susceptibility (TFS) Diagram can be generated using published values from ASME B1.1 to determine the minimum DTI needed for a bolt of any given diameter to meet the criterion of Hsr ≥ 1.2. The TFS diagram plots a material's DTI versus the size of a bolt and graphically delineates if a given bolt will experience notch strengthening (ductile behavior) or notch weakening (brittle behavior). For each bolt diameter, the minimum DTI needed for a bolt of a given size to meet an Hsr of 1.2 is calculated and plotted using the equation shown above. Since the geometry factor, Y, and the thread depth are both functions of the major and minor diameter, the minimum DTI needed to achieve an Hsr of 1.2 can be calculated using only data provided in ASME B1.1.

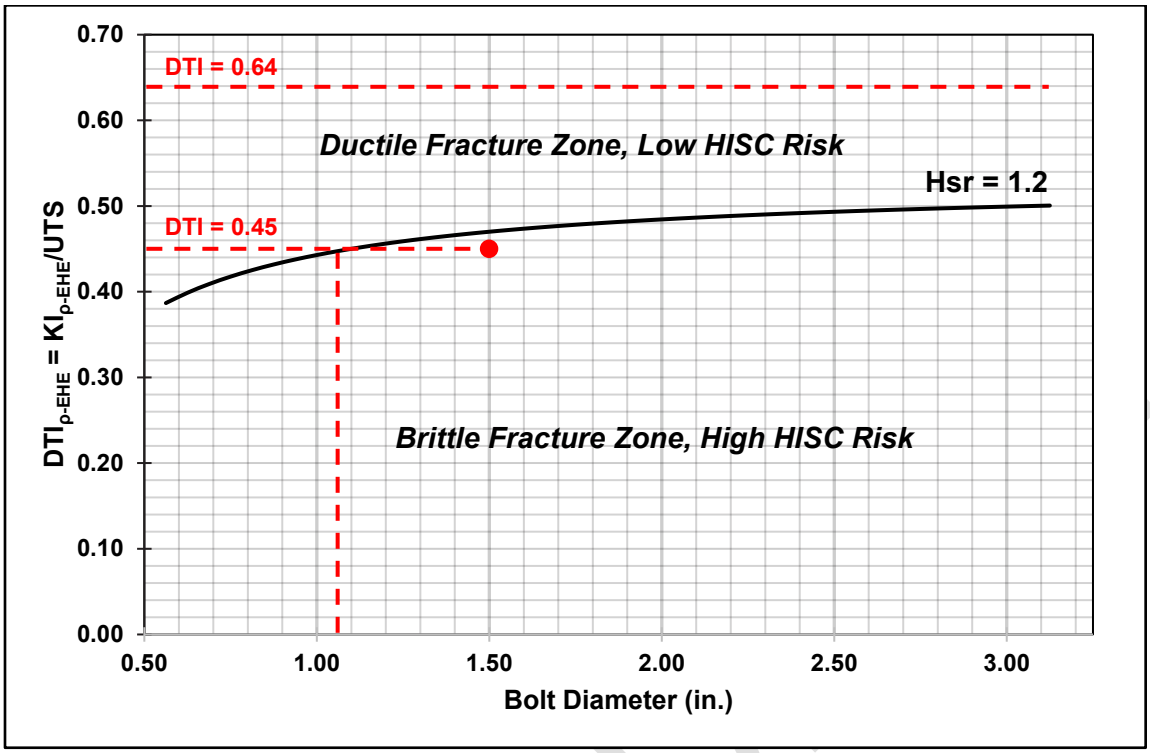

Figure B.2-Thread Fracture Susceptibility (TFS) Diagram for a 12-UNR threaded fastener under simulated CP

As seen in Figure B.2, a 1.5 in. (38.1 mm) diameter bolt made from the selected alloy 725 would not meet the minimum criterion of Hsr ≥ 1.2 to ensure that the bolt will experience yielding before brittle failure due to EHE. Following the Hsr = 1.2 trendline, the maximum diameter possible for the selected alloy ($DTI_{\rho\text{-}EHE}$ = 0.45) would be 1.0625" (27.0 mm) as shown by the vertical dashed line.

Further to the example, if YS had been used to calculate DTI, a $DTI_{\rho\text{-}EHE}$ of 0.64 would have resulted. All bolt diameters at this DTI value would meet or exceed the Hsr = 1.2 criteria for resistance to brittle fracture by HISC. Therefore, choice of DTI and Hsr calculation parameters is essential to proper assessment.

Figure B.2 shows that larger bolts require larger DTI values to avoid brittle fracture zone, which can initially appear counterintuitive. Further, the slope of curve is highly dependent on the thread type used. Based on results of testing, a thread with a minimum controlled root radius is recommended to minimize stress intensity at any given bolt diameter.

Bibliography

The following list of referenced documents provide helpful guidance and supporting information as related to the content of this Technical Report. Some referenced documents have been directly cited in this technical report for clarity.

[1] Raymond, L. “Accelerated Low Cost Test Method for Measuring the Susceptibility of HY-Steels to Hydrogen Embrittlement.” Current Solutions to Hydrogen Problems in Steels: Proceedings of the First International Conference on Current Solutions to Hydrogen Problems in Steels, 1982, pp.477-480.

[2] CF. Tiffany and J.N. Masters, “Applied Fracture Mechanics.” ASTM STP 381, 1964. PP 249-264.

[3] Hayden, M.J. “Incorporation of Residual Stress Effects in a Plasticity and Ductile Fracture Model for Reliability Assessments of Aluminum Ship Structure.” Ship Structure Committee, SSC-467, 2013.

[4] ASTM 2078, Standard Terminology Relating to Hydrogen Embrittlement Testing.

[5] Klier, EP. “The Effect of a Fatigue Crack on the Notch Strength and Fracture Development in Cylindrical Specimens of Heat Treated 4340 Steel.” U.S. Naval Research Laboratory, Washington D.C., 1963.

[6] Agogina, A. “Notch Effects, Stress State, and Ductility.” Journal of Engineering Materials and Technology, 1987. pp. 348-355.

[7] Raymond, L. “Handbook of Bolts and Bolted Joints—Chapter 39: The Susceptibility of Fasteners to Hydrogen Embrittlement and Stress Corrosion Cracking”. edited by John H. Bickford and Sayed Nassar (M. Dekker, New York, 1998), pp. 723-756.

[8] Raymond, L. “Acceptance Criterion for Hydrogen Embrittlement Testing of Coated Fasteners.” ASETSDefense 2009: Sustainable Surface Engineering for Aerospace and Defense Workshop. September 2009, Westminster, CO.

[9] S. McCoy, B. Baker, W. MacDonald, “Hydrogen Stress Cracking Resistance of Precipitation Hardenable Nickel Alloys and Optimization”, AMPP Annual Conference + Expo 2024, Paper No. 20719, New Orleans, LA, 2024.

[10] Barsom and Rolfe, “Fracture and Fatigue Control in Structures.” Prentice-Hall, Inc., 1977. pp. 98-102.

[11] Hertzberg, R. “Deformation and Fracture Mechanics of Engineering Materials.” John Wiley and Sons., 1976. pp. 236-284.

[12] Tada, H. “The Stress Analysis of Cracks Handbook.” Paris Productions, Inc. 1985.

[13] ASTM E399, *Standard Test Method for Linear-Elastic Plane-Strain Fracture Toughness of Metallic Materials*

[14] W.S.Pellini, “Advances in Fracture Toughness Characterization Procedures and in Quantitative Interpretations to Fracture-Safe Design for Structural Steels”, NRL Report 6713, Naval Research Laboratory. April 3, 1968.

[15] W.S.Pellini and P.P.Puzak, “Fracture Analysis Diagram Procedures for the Fracture-Safe Engineering Design of Steel structures.” Welding Research Council Bulletin 88. May 1963.

[16] CALTRANS – Bay Area Toll Authority, Toll Bridge Program Oversight Committee. “Report on the A354 Grade BD High-Strength Steel Rods on the New East Span of the San Francisco-Oakland Bay Bridge, With Findings and Decisions.” Commissioned Study. Metropolitan Transportation Commission Digital Library. 2013.

[17] API 6ACRA 1st Edition, *Age-hardened Nickel-based Alloys for Oil and Gas Drilling and Production Equipment*

[18] ASTM A354, *Standard Specification for Quenched and Tempered Alloy Steel Bolts, Studs, and Other Externally Threaded Fasteners*

[19] ASTM E8, *Standard Test Methods for Tension Testing of Metallic Materials*

[20] ASTM E18, *Standard Test Methods for Rockwell Hardness of Metallic Materials*

[21] ASTM E384, *Standard Test Method for Microindentation Hardness of Materials*

[22] ASTM E407, *Standard Practice for Microetching Metals and Alloys*

[23] ASTM E1290, *Standard Test Method for Crack-Tip Opening Displacement (CTOD) Fracture Toughness Measurement*

[24] ASTM E1820, *Standard Test Method for Measurement of Fracture Toughness*

[25] ASTM F519, *Standard Test Method for Process Control Verification to Prevent Hydrogen Embrittlement in Plated or Coated Fasteners*

[26] ASTM F1624, *Standard Test Method for Measurement of Hydrogen Embrittlement Threshold in Steel by the Incremental Step Loading Technique*